

An energy-stable parametric finite element method for anisotropic surface diffusion

Yifei Li^a, Weizhu Bao^{a,*}

^a*Department of Mathematics, National University of Singapore, Singapore, 119076*

Abstract

We propose an energy-stable parametric finite element method (ES-PFEM) to discretize the motion of a closed curve under surface diffusion with an anisotropic surface energy $\gamma(\theta)$ – anisotropic surface diffusion – in two dimensions, while θ is the angle between the outward unit normal vector and the vertical axis. By introducing a positive definite surface energy (density) matrix $G(\theta)$, we present a new and simple variational formulation for the anisotropic surface diffusion and prove that it satisfies area/mass conservation and energy dissipation. The variational problem is discretized in space by the parametric finite element method and area/mass conservation and energy dissipation are established for the semi-discretization. Then the problem is further discretized in time by a (semi-implicit) backward Euler method so that only a linear system is to be solved at each time step for the full-discretization and thus it is efficient. We establish well-posedness of the full-discretization and identify some simple conditions on $\gamma(\theta)$ such that the full-discretization keeps energy dissipation and thus it is unconditionally energy-stable. Finally the ES-PFEM is applied to simulate solid-state dewetting of thin films with anisotropic surface energies, i.e. the motion of an open curve under anisotropic surface diffusion with proper boundary conditions at the two triple points moving along the horizontal substrate. Numerical results are reported to demonstrate the efficiency and accuracy as well as energy dissipation of the proposed ES-PFEM.

Keywords: Anisotropic surface diffusion, anisotropic surface energy, parametric finite element method, energy-stable, solid-state dewetting

1. Introduction

Surface diffusion is a general and important process involving the motion of adatoms, atomic clusters (adparticles), and molecules at material surfaces and interfaces in solids [23]. It is an important mechanism and/or kinetics in epitaxial growth, surface phase formation, heterogeneous catalysis, and other areas in surface/materials science [25]. Due to different surface lattice orientations at material surface in solids, orientational anisotropy is a general pattern in both diffusion rates and mechanisms at the various surface orientations of a given material. This orientational anisotropy causes anisotropic surface energy and thus generates **anisotropic surface diffusion** at material surfaces and interfaces in solids [23, 28]. In fact, surface/anisotropic surface diffusion has manifested broader and significant applications in materials science and solid-state physics as well as computational geometry, such as crystal growth of nanomaterials [11], morphology development in alloys, evolution of voids in microelectronic circuits [21], solid-state dewetting [17, 26, 28–30], deformation of images [13], etc.

The mathematical model for surface diffusion in materials science can be traced back to the work by Mullins [22] for describing the diffusion at interfaces in alloys. Later, Davi and Gurtin [14] extended the model to anisotropic surface diffusion. By introducing the weighted mean curvature, Cahn and Taylor [12, 27]

*Corresponding author.

Email addresses: e0444158@u.nus.edu (Yifei Li), matbaowz@nus.edu.sg (Weizhu Bao)

proposed a simple mathematical model and showed that it is equivalent to the model in the literature for the anisotropic surface diffusion. For more details, we refer [4, 11, 19, 20] and references therein.

As illustrated in Figure 1, let $\Gamma := \Gamma(t)$ be a closed curve in two dimensions (2D), which is represented by $\mathbf{X} := \mathbf{X}(s, t) = (x(s, t), y(s, t))^T \in \mathbb{R}^2$ with t denoting the time and s being the arc length parametrization of Γ . The motion of Γ under anisotropic surface diffusion is governed by the following geometric partial differential equation (PDE) [4, 12, 19]:

$$\partial_t \mathbf{X} = \partial_{ss} \mu \mathbf{n}, \quad (1.1)$$

where $\tau = (\cos \theta, \sin \theta)^T$ is the unit tangent vector, $\mathbf{n} = (-\sin \theta, \cos \theta)^T$ is the outward unit normal vector with θ being the angle between \mathbf{n} and the vertical axis, and $\mu := \mu(s, t)$ is the weighted mean curvature (or chemical potential) defined as [4, 12, 19]:

$$\mu = [\gamma(\theta) + \gamma''(\theta)] \kappa, \quad (1.2)$$

with $\kappa := -(\partial_{ss} \mathbf{X}) \cdot \mathbf{n}$ being the curvature and $\gamma(\theta) \in C^2([-\pi, \pi])$ being the surface energy, which is a dimensionless positive and periodic function satisfying $\gamma(-\pi) = \gamma(\pi)$ and $\gamma'(-\pi) = \gamma'(\pi)$. The initial data for (1.1) is given as

$$\mathbf{X}(s, 0) = \mathbf{X}_0(s) = (x_0(s), y_0(s))^T, \quad 0 \leq s \leq L_0, \quad (1.3)$$

where L_0 is the length of the initial curve $\Gamma_0 = \Gamma(0)$.

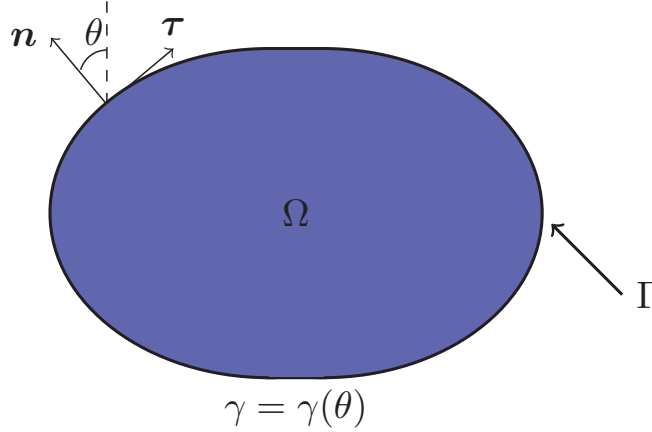


Figure 1: An illustration of a closed curve Γ in two dimensions under anisotropic surface diffusion with an anisotropic surface energy $\gamma(\theta)$, while θ is the angle between the outward unit normal vector \mathbf{n} and the y -axis.

Since $\Gamma(t)$ is parameterized by the arc length parameter s , the tangential vector τ and the outward unit normal vector \mathbf{n} can be expressed as

$$\tau = \partial_s \mathbf{X} = (\partial_s x, \partial_s y)^T, \quad \mathbf{n} = -\tau^\perp = -\partial_s \mathbf{X}^\perp = (-\partial_s y, \partial_s x)^T, \quad \partial_s x = \cos \theta, \quad \partial_s y = \sin \theta. \quad (1.4)$$

In addition, the curvature κ can also be formulated by s and θ as

$$\kappa = -(\partial_{ss} \mathbf{X}) \cdot \mathbf{n} = \partial_{ss} x \partial_s y - \partial_{ss} y \partial_s x = -(\sin^2 \theta + \cos^2 \theta) \partial_s \theta = -\partial_s \theta. \quad (1.5)$$

When $\gamma(\theta) \equiv 1$ for $\theta \in [-\pi, \pi]$, it is called as *isotropic* surface energy; and in this case, $\mu = \kappa$ in (1.2), and (1.1) is for surface diffusion [5, 6, 18, 22]. On the contrary, when $\gamma(\theta)$ is not a constant function, it is called as *anisotropic* surface energy; and in this case, μ is called as the weighted mean curvature (or chemical potential), and (1.1) is for anisotropic surface diffusion [20, 27]. In addition, when $\tilde{\gamma}(\theta) := \gamma(\theta) + \gamma''(\theta) > 0$

for $\theta \in [-\pi, \pi]$, i.e. the surface stiffness $\tilde{\gamma}(\theta)$ does not change sign, it is called as *weakly anisotropic*; and when $\tilde{\gamma}(\theta)$ changes sign for $\theta \in [-\pi, \pi]$, it is called as *strongly anisotropic*. In this paper, we assume that $\gamma(\theta)$ is isotropic/weakly anisotropic, i.e. $\gamma(\theta) + \gamma''(\theta) > 0$ for $\theta \in [-\pi, \pi]$. Typical anisotropic surface energy $\gamma(\theta)$ in materials science includes:

(i) the k -fold anisotropy surface energy [3]

$$\gamma(\theta) = 1 + \beta \cos(k(\theta - \theta_0)), \quad \theta \in [-\pi, \pi], \quad (1.6)$$

where $k = 2, 3, 4, 6$, β is the dimensionless anisotropic strength constant and $\theta_0 \in [-\pi, \pi]$ is a constant;

(ii) the ellipsoidal anisotropy surface energy [27]

$$\gamma(\theta) = \sqrt{a + b \cos^2 \theta}, \quad \theta \in [-\pi, \pi], \quad (1.7)$$

where a and b are two dimensionless constants satisfying $a > 0$ and $a + b > 0$; and

(iii) the Riemannian metric anisotropy surface energy [9]

$$\gamma(\theta) = \sum_{k=1}^K \sqrt{\mathbf{n}(\theta)^T G_k \mathbf{n}(\theta)}, \quad \text{with } \mathbf{n}(\theta) = (-\sin \theta, \cos \theta)^T, \quad \theta \in [-\pi, \pi], \quad (1.8)$$

where K is a positive integer, and $G_k \in \mathbb{R}^{2 \times 2}$ ($k = 1, 2, \dots, K$) are symmetric positive definite matrices. We remark here that when $K = 1$ and $G_1 = \text{diag}(a, b + a)$ in (1.8), then the Riemannian metric anisotropy surface energy (1.8) collapses to the ellipsoidal anisotropy surface energy (1.7).

Let $A(t)$ be the area/mass of the film (i.e., the region $\Omega(t)$ enclosed by the curve $\Gamma(t)$) and $W_c(t)$ be the total interfacial free energy, which are defined as

$$A(t) := \int_{\Omega(t)} 1 \, d\mathbf{x} = \int_0^{L(t)} y(s, t) \partial_s x(s, t) \, ds, \quad W_c(t) := \int_{\Gamma(t)} \gamma(\theta) \, ds = \int_0^{L(t)} \gamma(\theta) \, ds, \quad t \geq 0, \quad (1.9)$$

where $L(t) := \int_{\Gamma(t)} 1 \, ds$ is the length of $\Gamma(t)$, one can prove that [3, 4, 7]

$$\frac{d}{dt} A(t) = 0, \quad \frac{d}{dt} W_c(t) = - \int_0^{L(t)} (\partial_s \mu)^2 \, ds \leq 0, \quad t \geq 0, \quad (1.10)$$

which immediately implies the anisotropic surface diffusion (1.1)-(1.2) with (1.3) satisfies area/mass conservation and energy dissipation, i.e.

$$A(t) \equiv A(0) = \int_0^{L_0} y_0(s) x'_0(s) \, ds, \quad W_c(t) \leq W_c(t_1) \leq W_c(0) = \int_{\Gamma_0} \gamma(\theta) \, ds, \quad t \geq t_1 \geq 0. \quad (1.11)$$

For the surface diffusion, i.e. $\gamma(\theta) \equiv 1$ in (1.2), by reformulating (1.1)-(1.2) with $\gamma(\theta) \equiv 1$ into

$$\begin{cases} \mathbf{n} \cdot \partial_t \mathbf{X} - \partial_{ss} \kappa = 0, \\ \kappa \mathbf{n} + \partial_{ss} \mathbf{X} = 0, \end{cases} \quad 0 < s < L(t), \quad t > 0, \quad (1.12a)$$

$$(1.12b)$$

Barrett *et al.* [6, 7, 10] introduced a novel variational formulation of (1.12) and presented an elegant parametric finite element method (PFEM) for the evolution of a closed curve under surface diffusion. The PFEM has a few good properties including unconditional stability, energy dissipation and asymptotic mesh equal distribution (AMED). The proposed PFEM was successfully extended for simulating the anisotropic surface diffusion with the specific Riemannian metric anisotropy surface energy (1.8) by adapting a variational formation of (1.1)-(1.2) via the anisotropic surface energy γ in terms of $\gamma(\mathbf{n})$ instead of $\gamma(\theta)$ by Barrett *et al.* [9]. The PFEM was also extended for solving the anisotropic surface diffusion with applications in simulating solid-state dewetting by reformulating (1.1)-(1.2) into

$$\begin{cases} \mathbf{n} \cdot \partial_t \mathbf{X} - \partial_{ss} \mu = 0, \\ \mu = [\gamma(\theta) + \gamma''(\theta)] \kappa, \\ \kappa \mathbf{n} + \partial_{ss} \mathbf{X} = 0, \end{cases} \quad 0 < s < L(t), \quad t > 0, \quad (1.13a)$$

$$(1.13b)$$

$$(1.13c)$$

and obtaining a variational formulation with $(\mathbf{X}, \mu, \kappa)$ as unknown functions [3]. Unfortunately those good properties of the PFEM for surface diffusion, such as unconditional stability, energy dissipation and asymptotic mesh equal distribution, are lost in the above extension for general anisotropic surface diffusion [3].

The main aim of this paper is to present a new and simple variational formulation for the anisotropic surface diffusion (1.1)-(1.2) with (\mathbf{X}, μ) as unknown functions by introducing an anisotropic surface energy matrix $G(\theta)$ depending on $\gamma(\theta)$. An energy-stable parametric finite element method (ES-PFEM) is then proposed for the discretization of the new variational problem under some simple conditions on $\gamma(\theta)$. The proposed ES-PFEM for anisotropic surface diffusion enjoys most good properties of the original PFEM for surface diffusion, such as semi-implicit and thus efficient, unconditional stability, energy dissipation and asymptotic mesh quasi-equal distribution. The proposed ES-PFEM is extended to simulate solid-state dewetting, i.e. the motion of an open curve under anisotropic surface diffusion and contact line migration [31].

The rest of the paper is organized as follows: In section 2, we present a new and simple variational formulation and prove its area/mass conservation and energy dissipation. In section 3, we propose a semi-discretization in space by PFEM for the variational problem and show its area/mass conservation and energy dissipation. In section 4, we present a full-discretization by adapting a (semi-implicit) backward Euler method in time, establish well-posedness of the full-discretization and identify some simple conditions on $\gamma(\theta)$ such that the full-discretization is energy dissipative. Extension of the ES-PFEM to simulate solid-state dewetting of thin films under anisotropic surface diffusion and contact line migration is presented in section 5. Numerical results are reported in section 6 to demonstrate the efficiency, accuracy and unconditional energy stability of the proposed ES-PFEM. Finally, some conclusions are drawn in section 7.

2. A new variational formulation and its properties

In this section, we present a new and simple variational formulation for the anisotropic surface diffusion (1.1)-(1.2) and establish its area/mass conservation and energy dissipation.

2.1. The new formulation

Similar to (1.12) for the surface diffusion, we reformulate the anisotropic surface diffusion (1.1)-(1.2) for the evolution of a closed curve as

$$\begin{cases} \mathbf{n} \cdot \partial_t \mathbf{X} - \partial_{ss} \mu = 0, & 0 < s < L(t), & t > 0, \end{cases} \quad (2.1a)$$

$$\mu \mathbf{n} + [\gamma(\theta) + \gamma''(\theta)] \partial_{ss} \mathbf{X} = 0. \quad (2.1b)$$

In order to obtain a variational formulation of (2.1), for convenience, we introduce a time independent variable ρ such that $\Gamma(t)$ can be parameterized over the fixed domain $\rho \in \mathbb{I} = [0, 1]$ (here ρ and s can be respectively regarded as the Lagrangian and Eulerian variables of the closed curve $\Gamma(t)$, and we do not distinguish $\mathbf{X}(\rho, t)$ and $\mathbf{X}(s, t)$ for representing $\Gamma(t)$ when there is no misunderstanding) as

$$\Gamma(t) := \mathbf{X}(\rho, t) = (x(\rho, t), y(\rho, t))^T : \mathbb{I} \times [0, T] \rightarrow \mathbb{R}^2. \quad (2.2)$$

Based on this parametrization, the arc length parameter s can be given as $s(\rho, t) = \int_0^\rho |\partial_q \mathbf{X}| dq$, and we have $\partial_\rho s = |\partial_\rho \mathbf{X}|$, $ds = \partial_\rho s d\rho = |\partial_\rho \mathbf{X}| d\rho$. We also introduce the functional space with respect to the evolution of the closed curve $\Gamma(t)$ as

$$L^2(\mathbb{I}) = \left\{ u : \mathbb{I} \rightarrow \mathbb{R} \mid \int_{\Gamma(t)} |u(s)|^2 ds = \int_{\mathbb{I}} |u(s(\rho, t))|^2 \partial_\rho s d\rho < +\infty \right\}, \quad (2.3)$$

equipped with the L^2 -inner product

$$(u, v)_{\Gamma(t)} := \int_{\Gamma(t)} u(s) v(s) ds = \int_{\mathbb{I}} u(s(\rho, t)) v(s(\rho, t)) \partial_\rho s d\rho, \quad \forall u, v \in L^2(\mathbb{I}). \quad (2.4)$$

Extension of (2.4) to $L^2(\mathbb{I})^2$ is straightforward. Moreover, define the Sobolev spaces

$$\begin{aligned}\mathbb{K} &:= H^1(\mathbb{I}) = \{u : \mathbb{I} \rightarrow \mathbb{R} \mid u \in L^2(\mathbb{I}), \partial_\rho u \in L^2(\mathbb{I})\}, \\ \mathbb{K}_p &:= H_p^1(\mathbb{I}) = \{u \in H^1(\mathbb{I}) \mid u(0) = u(1)\}, \quad \mathbb{X}_p := H_p^1(\mathbb{I}) \times H_p^1(\mathbb{I}).\end{aligned}$$

In addition, for a vector $\mathbf{v} = (v_1, v_2)^T \in \mathbb{R}^2$, we denote $\mathbf{v}^\perp \in \mathbb{R}^2$ as its perpendicular vector (rotation clockwise by $\pi/2$) defined as

$$\mathbf{v}^\perp := (v_2, -v_1)^T = -J \mathbf{v}, \quad \text{with } J = \begin{pmatrix} 0 & -1 \\ 1 & 0 \end{pmatrix}, \quad (2.5)$$

which immediately implies that

$$(\mathbf{v}^\perp)^\perp = -J \mathbf{v}^\perp = J^2 \mathbf{v} = -\mathbf{v}, \quad \mathbf{v} = (v_1, v_2)^T \in \mathbb{R}^2. \quad (2.6)$$

Multiplying a test function $\varphi(\rho) \in \mathbb{K}_p$ to (2.1a) and then integrating over $\Gamma(t)$, integrating by parts, noting $\partial_s \mu(0, t) = \partial_s \mu(1, t)$ and $\varphi(0) = \varphi(1)$, we have

$$\begin{aligned}\left(\partial_t \mathbf{X}, \varphi \mathbf{n}\right)_{\Gamma(t)} &= \left(\mathbf{n} \cdot \partial_t \mathbf{X}, \varphi\right)_{\Gamma(t)} = \left(\partial_{ss} \mu, \varphi\right)_{\Gamma(t)} \\ &= -\left(\partial_s \mu, \partial_s \varphi\right)_{\Gamma(t)} + (\varphi \partial_s \mu)|_{\rho=0}^{\rho=1} \\ &= -\left(\partial_s \mu, \partial_s \varphi\right)_{\Gamma(t)}.\end{aligned} \quad (2.7)$$

To get the variational formulation of (2.1b), noticing $\kappa = -\partial_s \theta$ in (1.5), we have

$$\partial_s \gamma(\theta) = \gamma'(\theta) \partial_s \theta = -\kappa \gamma'(\theta), \quad \partial_s \gamma'(\theta) = \gamma''(\theta) \partial_s \theta = -\kappa \gamma''(\theta), \quad \theta \in [-\pi, \pi]. \quad (2.8)$$

Combining (1.4) and (2.6) with $\mathbf{v} = \boldsymbol{\tau}$, and noticing $\kappa \mathbf{n} = -\partial_{ss} \mathbf{X}$, we obtain

$$\kappa \partial_s \mathbf{X} = \kappa \boldsymbol{\tau} = -\kappa (\boldsymbol{\tau}^\perp)^\perp = \kappa (-\boldsymbol{\tau}^\perp)^\perp = \kappa \mathbf{n}^\perp = -\partial_{ss} \mathbf{X}^\perp, \quad \kappa \partial_s \mathbf{X}^\perp = -\kappa \mathbf{n} = \partial_{ss} \mathbf{X}. \quad (2.9)$$

Plugging (2.8) into (2.1b), noting (2.9), we get

$$\begin{aligned}\mu \mathbf{n} &= -[\gamma(\theta) + \gamma''(\theta)] \partial_{ss} \mathbf{X} \\ &= \partial_s (-\gamma(\theta) \partial_s \mathbf{X}) + \partial_s \gamma(\theta) \partial_s \mathbf{X} - \gamma''(\theta) \kappa \partial_s \mathbf{X}^\perp \\ &= \partial_s (-\gamma(\theta) \partial_s \mathbf{X}) - \kappa \gamma'(\theta) \partial_s \mathbf{X} + \gamma''(\theta) \partial_s \theta \partial_s \mathbf{X}^\perp \\ &= \partial_s (-\gamma(\theta) \partial_s \mathbf{X}) + \gamma'(\theta) \partial_{ss} \mathbf{X}^\perp + \partial_s \gamma'(\theta) \partial_s \mathbf{X}^\perp \\ &= \partial_s (-\gamma(\theta) \partial_s \mathbf{X} + \gamma'(\theta) \partial_s \mathbf{X}^\perp).\end{aligned} \quad (2.10)$$

Introducing the surface energy (density) matrix $G(\theta)$ as

$$G(\theta) = \begin{pmatrix} \gamma(\theta) & -\gamma'(\theta) \\ \gamma'(\theta) & \gamma(\theta) \end{pmatrix}, \quad (2.11)$$

and noting (2.5) with $\mathbf{v} = \partial_s \mathbf{X}$, we have

$$-\gamma(\theta) \partial_s \mathbf{X} + \gamma'(\theta) \partial_s \mathbf{X}^\perp = -[\gamma(\theta) \partial_s \mathbf{X} - \gamma'(\theta) \partial_s \mathbf{X}^\perp] = -[\gamma(\theta) I_2 + \gamma'(\theta) J] \partial_s \mathbf{X} = -G(\theta) \partial_s \mathbf{X}, \quad (2.12)$$

where I_2 is the 2×2 identity matrix. Substituting (2.12) into (2.10), we obtain

$$\mu \mathbf{n} = -\partial_s (G(\theta) \partial_s \mathbf{X}). \quad (2.13)$$

Thus (2.1) (or (1.1)-(1.2)) is equivalent to the following conservative form:

$$\begin{cases} \mathbf{n} \cdot \partial_t \mathbf{X} - \partial_{ss} \mu = 0, & 0 < s < L(t), & t > 0, \\ \mu \mathbf{n} + \partial_s (G(\theta) \partial_s \mathbf{X}) = 0. \end{cases} \quad (2.14a)$$

Multiplying a test function $\boldsymbol{\omega} = (\omega_1, \omega_2)^T \in \mathbb{X}_p$ to (2.1b) and then integrating over $\Gamma(t)$, noticing (2.13) and integrating by parts, noting $\theta(0, t) = \theta(1, t)$, $G(\theta(0, t)) = G(\theta(1, t))$, $\partial_s \mathbf{X}(0, t) = \partial_s \mathbf{X}(1, t)$ and $\boldsymbol{\omega}(0) = \boldsymbol{\omega}(1)$, we get

$$\begin{aligned} (\mu, \mathbf{n} \cdot \boldsymbol{\omega})_{\Gamma(t)} &= (\mu \mathbf{n}, \boldsymbol{\omega})_{\Gamma(t)} = (-\partial_s (G(\theta) \partial_s \mathbf{X}), \boldsymbol{\omega})_{\Gamma(t)} \\ &= (G(\theta) \partial_s \mathbf{X}, \partial_s \boldsymbol{\omega})_{\Gamma(t)} + ((-G(\theta) \partial_s \mathbf{X}) \cdot \boldsymbol{\omega})|_{\rho=0}^{\rho=1} \\ &= (G(\theta) \partial_s \mathbf{X}, \partial_s \boldsymbol{\omega})_{\Gamma(t)}. \end{aligned} \quad (2.15)$$

Combining (2.7) and (2.15), we get a new and simple variational formulation for the anisotropic surface diffusion (1.1)-(1.2) with the initial condition (1.3) as: Given the initial curve $\Gamma(0) := \mathbf{X}(\rho, 0) = \mathbf{X}_0(L_0 \rho) \in \mathbb{X}_p$, find the solution $\Gamma(t) := \mathbf{X}(\cdot, t) \in \mathbb{X}_p$ and $\mu(t) \in \mathbb{K}_p$ such that:

$$(\partial_t \mathbf{X}, \varphi \mathbf{n})_{\Gamma(t)} + (\partial_s \mu, \partial_s \varphi)_{\Gamma(t)} = 0, \quad \forall \varphi \in \mathbb{K}_p, \quad (2.16a)$$

$$(\mu, \mathbf{n} \cdot \boldsymbol{\omega})_{\Gamma(t)} - (G(\theta) \partial_s \mathbf{X}, \partial_s \boldsymbol{\omega})_{\Gamma(t)} = 0, \quad \forall \boldsymbol{\omega} \in \mathbb{X}_p. \quad (2.16b)$$

2.2. Area/mass conservation and energy dissipation

Assume that the anisotropic surface energy $\gamma(\theta) \in C^1([-\pi, \pi])$ and $\gamma(-\pi) = \gamma(\pi)$, for the variational problem (2.16), we have

Proposition 2.1 (area/mass conservation and energy dissipation). *Let $(\mathbf{X}(\cdot, t), \mu(\cdot, t)) \in \mathbb{X}_p \times \mathbb{K}_p$ be a solution of the variational problem (2.16). Then the area/mass $A(t)$ defined in (1.9) is conserved and the total interfacial energy $W_c(t)$ defined in (1.9) is dissipative, i.e. (1.11) is valid.*

Proof. Differentiating $A(t)$ defined in (1.9) with respect to t , integrating by parts, we get

$$\begin{aligned} \frac{d}{dt} A(t) &= \frac{d}{dt} \int_0^{L(t)} y(s, t) \partial_s x(s, t) ds \\ &= \frac{d}{dt} \int_0^1 y(\rho, t) \partial_\rho x(\rho, t) d\rho = \int_0^1 (\partial_t y \partial_\rho x + y \partial_t \partial_\rho x) d\rho \\ &= \int_0^1 (\partial_t y \partial_\rho x - \partial_\rho y \partial_t x) d\rho + (y \partial_t x)|_{\rho=0}^{\rho=1} \\ &= \int_{\Gamma(t)} (\partial_t \mathbf{X}) \cdot \mathbf{n} ds = (\partial_t \mathbf{X}, \mathbf{n})_{\Gamma(t)}, \quad t \geq 0. \end{aligned} \quad (2.17)$$

Taking $\varphi \equiv 1$ in (2.16a), we have

$$(\partial_t \mathbf{X}, \mathbf{n})_{\Gamma(t)} = -(\partial_s \mu, \partial_s 1)_{\Gamma(t)} = -(\partial_s \mu, 0)_{\Gamma(t)} = 0, \quad t \geq 0. \quad (2.18)$$

Inserting (2.18) into (2.17), we obtain

$$\frac{d}{dt} A(t) = 0, \quad t \geq 0, \quad (2.19)$$

which immediately implies the area/mass conservation in (1.11).

Similar to (1.5), we obtain

$$\partial_t \theta = (\sin^2 \theta + \cos^2 \theta) \partial_t \theta = -\partial_s \partial_t x \partial_s y + \partial_s \partial_t y \partial_s x = -(\partial_s \partial_t \mathbf{X}) \cdot (\partial_s \mathbf{X}^\perp). \quad (2.20)$$

Differentiating $W_c(t)$ defined in (1.9) with respect to t , noting (2.20), we get

$$\begin{aligned} \frac{d}{dt} W_c(t) &= \frac{d}{dt} \int_0^{L(t)} \gamma(\theta) ds = \frac{d}{dt} \int_0^1 \gamma(\theta) \partial_\rho s d\rho \\ &= \int_0^1 (\gamma(\theta) \partial_t \partial_\rho s + \gamma'(\theta) \partial_t \theta \partial_\rho s) d\rho \\ &= \int_0^1 (\gamma(\theta) \partial_s \mathbf{X} \cdot \partial_s \partial_t \mathbf{X} - \gamma'(\theta) \partial_s \mathbf{X}^\perp \cdot \partial_s \partial_t \mathbf{X}) \partial_\rho s d\rho \\ &= \left(G(\theta) \partial_s \mathbf{X}, \partial_s \partial_t \mathbf{X} \right)_{\Gamma(t)}, \quad t \geq 0. \end{aligned} \quad (2.21)$$

Taking the test functions $\varphi = \mu$ in (2.16a) and $\boldsymbol{\omega} = \partial_t \mathbf{X}$ in (2.16b), we obtain

$$\left(\partial_t \mathbf{X}, \mu \mathbf{n} \right)_{\Gamma(t)} = - \left(\partial_s \mu, \partial_s \mu \right)_{\Gamma(t)}, \quad \left(G(\theta) \partial_s \mathbf{X}, \partial_s \partial_t \mathbf{X} \right)_{\Gamma(t)} = \left(\mu \mathbf{n}, \partial_t \mathbf{X} \right)_{\Gamma(t)}, \quad t \geq 0. \quad (2.22)$$

Substituting (2.22) into (2.21), we have

$$\begin{aligned} \frac{d}{dt} W_c(t) &= \left(G(\theta) \partial_s \mathbf{X}, \partial_s \partial_t \mathbf{X} \right)_{\Gamma(t)} = \left(\mu \mathbf{n}, \partial_t \mathbf{X} \right)_{\Gamma(t)} \\ &= - \left(\partial_s \mu, \partial_s \mu \right)_{\Gamma(t)} \leq 0, \quad t \geq 0, \end{aligned} \quad (2.23)$$

which immediately implies the energy dissipation in (1.11). \square

3. A semi-discretization by PFEM and its properties

In this section, we present a parametric finite element method (PFEM) with conforming piecewise linear elements to discretize the variational problem (2.16) and show that the semi-discretization conserves area/mass and keeps energy dissipation.

3.1. The semi-discretization in space

Let $N > 2$ be a positive integer and $h = 1/N$ be the mesh size, denote the grid points $\rho_j = jh$ for $j = 0, 1, \dots, N$, and subintervals $I_j = [\rho_{j-1}, \rho_j]$ for $j = 1, 2, \dots, N$. Then a uniform partition of the interval \mathbb{I} is given as $\mathbb{I} = [0, 1] = \bigcup_{j=1}^N I_j$. Introduce the finite element subspaces

$$\begin{aligned} \mathbb{K}^h &:= \{u^h \in C(\mathbb{I}) \mid u^h|_{I_j} \in \mathcal{P}_1, \forall j = 1, 2, \dots, N\} \subset \mathbb{K}, \\ \mathbb{K}_p^h &:= \{u^h \in \mathbb{K}^h \mid u(0) = u(1)\} \subset \mathbb{K}_p, \quad \mathbb{X}_p^h := \mathbb{K}_p^h \times \mathbb{K}_p^h \subset \mathbb{X}_p, \end{aligned}$$

where \mathcal{P}_1 denotes the space of all polynomials with degree at most 1.

Let $\Gamma^h(t) := \mathbf{X}^h(\cdot, t) \in \mathbb{X}_p^h$ and $\mu^h(t) \in \mathbb{K}_p^h$ be the numerical approximations of the closed curve $\Gamma(t) := \mathbf{X}(\cdot, t) \in \mathbb{X}_p$ and $\mu(\cdot, t) \in \mathbb{K}_p$, respectively, which is the solution of the variational problem (2.16). In fact, for $t \geq 0$, the piecewise linear curve $\Gamma^h(t)$ is composed by ordered line segments $\{\mathbf{h}_j(t)\}_{j=1}^N$ and we always assume that they satisfy

$$h_{\min}(t) := \min_{1 \leq j \leq N} |\mathbf{h}_j(t)| > 0, \quad \text{with} \quad \mathbf{h}_j(t) := \mathbf{X}^h(\rho_j, t) - \mathbf{X}^h(\rho_{j-1}, t), \quad j = 1, 2, \dots, N, \quad (3.1)$$

where $|\mathbf{h}_j(t)|$ denotes the length of the vector $\mathbf{h}_j(t)$ for $j = 1, 2, \dots, N$. With the piecewise linear elements, it is easy to see that the unit tangential vector $\boldsymbol{\tau}^h$, the outward unit normal vector \mathbf{n}^h and the inclination angle θ^h of the curve $\Gamma^h(t)$ are constant vectors/scalars on each interval I_j with possible discontinuities or jumps at nodes ρ_j . In fact, for $1 \leq j \leq N$, the two vectors $\boldsymbol{\tau}^h$, \mathbf{n}^h on each interval I_j can be computed as

$$\boldsymbol{\tau}^h|_{I_j} = \frac{\mathbf{h}_j}{|\mathbf{h}_j|} := \boldsymbol{\tau}_j^h, \quad \mathbf{n}^h|_{I_j} = -(\boldsymbol{\tau}_j^h)^\perp = -\frac{(\mathbf{h}_j)^\perp}{|\mathbf{h}_j|} := \mathbf{n}_j^h; \quad (3.2)$$

and the angle θ^h on each interval I_j is

$$\theta^h|_{I_j} := \theta_j^h, \quad \text{satisfying} \quad \cos \theta_j^h = \frac{h_{j,x}}{|\mathbf{h}_j|}, \quad \sin \theta_j^h = \frac{h_{j,y}}{|\mathbf{h}_j|}, \quad \text{with} \quad \mathbf{h}_j = (h_{j,x}, h_{j,y})^T. \quad (3.3)$$

Furthermore, for two piecewise linear scalar (or vector) functions u and v defined on \mathbb{I} with possible jumps at the nodes $\{\rho_j\}_{j=0}^N$, we can define the mass lumped inner product $(\cdot, \cdot)_{\Gamma^h(t)}^h$ over $\Gamma^h(t)$ as

$$(u, v)_{\Gamma^h(t)}^h := \frac{1}{2} \sum_{j=1}^N |\mathbf{h}_j| \left[(u \cdot v)(\rho_j^-) + (u \cdot v)(\rho_{j-1}^+) \right], \quad (3.4)$$

where $u(\rho_j^\pm) = \lim_{\rho \rightarrow \rho_j^\pm} u(\rho)$ for $0 \leq j \leq N$.

Let $\Gamma^h(0) := \mathbf{X}^h(\rho, 0) \in \mathbb{X}_p^h$ be an interpolation of the initial curve $\mathbf{X}_0(s)$ in (1.3) satisfying $\mathbf{X}_0(0) = \mathbf{X}_0(L_0)$, which is defined as $\mathbf{X}^h(\rho = \rho_j, 0) = \mathbf{X}_0(s = s_j^0)$ with $s_j^0 = L_0 \rho_j$ for $j = 0, 1, \dots, N$. Then a semi-discretization in space of the variational formulation (2.16) can be given as: Take $\Gamma^h(0) = \mathbf{X}^h(\cdot, 0) \in \mathbb{X}_p^h$, find the closed curve $\Gamma^h(t) := \mathbf{X}^h(\cdot, t) = (x^h(\cdot, t), y^h(\cdot, t))^T \in \mathbb{X}_p^h$ and the weighted mean curvature $\mu^h(\cdot, t) \in \mathbb{K}_p^h$, such that

$$\left(\partial_t \mathbf{X}^h, \varphi^h \mathbf{n}^h \right)_{\Gamma^h(t)}^h + \left(\partial_s \mu^h, \partial_s \varphi^h \right)_{\Gamma^h(t)}^h = 0, \quad \forall \varphi^h \in \mathbb{K}_p^h, \quad (3.5a)$$

$$\left(\mu^h, \mathbf{n}^h \cdot \boldsymbol{\omega}^h \right)_{\Gamma^h(t)}^h - \left(G(\theta^h) \partial_s \mathbf{X}^h, \partial_s \boldsymbol{\omega}^h \right)_{\Gamma^h(t)}^h = 0, \quad \forall \boldsymbol{\omega}^h \in \mathbb{X}_p^h. \quad (3.5b)$$

3.2. Area/mass conservation and energy dissipation

Let $A^h(t)$ be the area/mass of the region enclosed by the closed curve $\Gamma^h(t)$ and $W_c^h(t)$ be its total interfacial energy, which are defined as

$$A^h(t) = \frac{1}{2} \sum_{j=1}^N (x_j(t) - x_{j-1}(t))(y_j(t) + y_{j-1}(t)), \quad W_c^h(t) = \sum_{j=1}^N |\mathbf{h}_j(t)| \gamma(\theta_j^h), \quad (3.6)$$

where $\mathbf{X}_j(t) = (x_j(t), y_j(t))^T := \mathbf{X}^h(\rho_j, t)$ for $j = 0, 1, \dots, N$. For the semi-discretization (3.5), we have

Proposition 3.1 (area/mass conservation and energy dissipation). *Let $(\mathbf{X}^h(\cdot, t), \mu^h(\cdot, t)) \in \mathbb{X}_p^h \times \mathbb{K}_p^h$ be a solution of the semi-discretization (3.5). Then the area/mass $A^h(t)$ in (3.6) is conserved, i.e.*

$$A^h(t) \equiv A^h(0) = \frac{1}{2} \sum_{j=1}^N [x_0(s_j^0) - x_0(s_{j-1}^0)][y_0(s_j^0) + y_0(s_{j-1}^0)], \quad t \geq 0; \quad (3.7)$$

and the total interfacial energy $W_c^h(t)$ in (3.6) is dissipative, i.e.

$$W_c^h(t) \leq W_c^h(t_1) \leq W_c^h(0) = \sum_{j=1}^N |\mathbf{h}_j(0)| \gamma(\theta_j^h(0)), \quad t \geq t_1 \geq 0. \quad (3.8)$$

Proof. The area/mass conservation (3.7) of the semi-discretization (3.5) can be proved similar to those in [3, Proposition 2.1] and thus the details are omitted here for brevity.

Similar to the proof of (2.20), noting (1.5) and (3.3), we obtain

$$\dot{\theta}_j^h(t) = (\sin^2(\theta_j^h) + \cos^2(\theta_j^h)) \dot{\theta}_j^h(t) = \frac{-\dot{h}_{j,x} h_{j,y} + \dot{h}_{j,y} h_{j,x}}{|\mathbf{h}_j|^2} = -\frac{\mathbf{h}_j^\perp \cdot \dot{\mathbf{h}}_j}{|\mathbf{h}_j|^2}. \quad (3.9)$$

Differentiating $W_c^h(t)$ in (3.6) with respect to t , noticing (2.12) and (3.9), we get

$$\begin{aligned} \frac{d}{dt} W_c^h(t) &= \frac{d}{dt} \left(\sum_{j=1}^N |\mathbf{h}_j(t)| \gamma(\theta_j^h) \right) = \sum_{j=1}^N \left(\gamma(\theta_j^h) \frac{d}{dt} |\mathbf{h}_j(t)| + \gamma'(\theta_j^h) \dot{\theta}_j^h |\mathbf{h}_j(t)| \right) \\ &= \sum_{j=1}^N \left(\gamma(\theta_j^h) \frac{\mathbf{h}_j(t) \cdot \dot{\mathbf{h}}_j(t)}{|\mathbf{h}_j(t)|} - \gamma'(\theta_j^h) \frac{\mathbf{h}_j(t)^\perp \cdot \dot{\mathbf{h}}_j(t)}{|\mathbf{h}_j(t)|} \right) \\ &= \sum_{j=1}^N |\mathbf{h}_j(t)| \left(\gamma(\theta_j^h) \frac{\mathbf{h}_j(t)}{|\mathbf{h}_j(t)|} - \gamma'(\theta_j^h) \frac{\mathbf{h}_j(t)^\perp}{|\mathbf{h}_j(t)|} \right) \cdot \frac{\dot{\mathbf{h}}_j(t)}{|\mathbf{h}_j(t)|} \\ &= \sum_{j=1}^N |\mathbf{h}_j(t)| \left(G(\theta^h) \frac{\mathbf{h}_j(t)}{|\mathbf{h}_j(t)|} \right) \cdot \frac{\dot{\mathbf{h}}_j(t)}{|\mathbf{h}_j(t)|} \\ &= \sum_{j=1}^N |\mathbf{h}_j(t)| \left(G(\theta^h) \partial_s \mathbf{X}^h|_{I_j} \right) \cdot (\partial_s \partial_t \mathbf{X}^h)|_{I_j} \\ &= \left(G(\theta^h) \partial_s \mathbf{X}^h, \partial_s \partial_t \mathbf{X}^h \right)_{\Gamma^h(t)}^h. \end{aligned} \quad (3.10)$$

Here we use the following equalities

$$\partial_s \mathbf{X}^h|_{I_j} = \frac{\mathbf{h}_j(t)}{|\mathbf{h}_j(t)|}, \quad \partial_s \partial_t \mathbf{X}^h|_{I_j} = \frac{1}{|\mathbf{h}_j(t)|} \partial_t \mathbf{X}^h|_{I_j} = \frac{\dot{\mathbf{h}}_j(t)}{|\mathbf{h}_j(t)|}, \quad 1 \leq j \leq N. \quad (3.11)$$

Choosing the test functions $\varphi^h = \mu^h$ in (3.5a) and $\omega^h = \partial_t \mathbf{X}^h$ in (3.5b), we have

$$\left(\partial_t \mathbf{X}^h, \mu^h \mathbf{n}^h \right)_{\Gamma^h(t)}^h = - \left(\partial_s \mu^h, \partial_s \mu^h \right)_{\Gamma^h(t)}^h, \quad \left(G(\theta^h) \partial_s \mathbf{X}^h, \partial_s \partial_t \mathbf{X}^h \right)_{\Gamma^h(t)}^h = \left(\mu^h \mathbf{n}^h, \partial_t \mathbf{X}^h \right)_{\Gamma^h(t)}^h. \quad (3.12)$$

Substituting (3.12) into (3.10), we get

$$\begin{aligned} \frac{d}{dt} W_c^h(t) &= \left(G(\theta^h) \partial_s \mathbf{X}^h, \partial_s \partial_t \mathbf{X}^h \right)_{\Gamma^h(t)}^h \\ &= \left(\mu^h \mathbf{n}^h, \partial_t \mathbf{X}^h \right)_{\Gamma^h(t)}^h = \left(\partial_t \mathbf{X}^h, \mu^h \mathbf{n}^h \right)_{\Gamma^h(t)}^h \\ &= - \left(\partial_s \mu^h, \partial_s \mu^h \right)_{\Gamma^h(t)}^h \leq 0, \quad t \geq 0, \end{aligned} \quad (3.13)$$

which immediately implies the energy dissipation in (3.8). \square

4. An energy-stable PFEM and its properties

In this section, we further discretize the semi-discretization (3.5) in time by a semi-implicit backward Euler method to obtain a full-discretization of the variational problem (2.16) (and thus of the original problem (2.1) or (1.1)-(1.2)), establish its well-posedness and investigate some simple conditions on $\gamma(\theta)$ such that the full-discretization is energy dissipative.

4.1. The full-discretization

Take $\tau > 0$ as the time step size and denote $t_m = m\tau$ the discrete time levels for $m = 0, 1, \dots$. For each $m \geq 0$, let $\Gamma^m := \mathbf{X}^m(\rho) = (x^m(\rho), y^m(\rho))^T \in \mathbb{X}_p^h$ and $\mu^m \in \mathbb{K}_p^h$ be the approximations of $\Gamma^h(t_m) = \mathbf{X}^h(\rho, t_m)$ and $\mu^h(t_m) \in \mathbb{K}_p^h$, respectively, which is the solution of the semi-discretization (3.5). Similarly, Γ^m is composed by segments $\{\mathbf{h}_j^m\}_{j=1}^N$ defined as

$$\mathbf{h}_j^m = (h_{j,x}^m, h_{j,y}^m)^T := \mathbf{X}^m(\rho_j) - \mathbf{X}^m(\rho_{j-1}), \quad j = 1, 2, \dots, N. \quad (4.1)$$

Again, the unit tangential vector $\boldsymbol{\tau}^m$, the outward unit normal vector \mathbf{n}^m and the inclination angle θ^m of the curve Γ^m are constant vectors/scalars on each interval I_j with possible discontinuities or jumps at nodes ρ_j ($j = 0, 1, \dots, N$). The two vectors $\boldsymbol{\tau}^m$ and \mathbf{n}^m on interval I_j can be computed as

$$\boldsymbol{\tau}^m|_{I_j} = \frac{\mathbf{h}_j^m}{|\mathbf{h}_j^m|} := \boldsymbol{\tau}_j^m, \quad \mathbf{n}^m|_{I_j} = -(\boldsymbol{\tau}_j^m)^\perp = -\frac{(\mathbf{h}_j^m)^\perp}{|\mathbf{h}_j^m|} := \mathbf{n}_j^m, \quad 1 \leq j \leq N, \quad (4.2)$$

and the angle θ^m on each interval I_j is given as

$$\theta^m|_{I_j} := \theta_j^m, \quad \text{satisfying} \quad \cos \theta_j^m = \frac{h_{j,x}^m}{|\mathbf{h}_j^m|}, \quad \sin \theta_j^m = \frac{h_{j,y}^m}{|\mathbf{h}_j^m|}, \quad 1 \leq j \leq N. \quad (4.3)$$

Then an energy-stable PFEM (**ES-PFEM**) to discretize the semi-discretization (3.5) is to adapt a semi-implicit backward Euler method in time and is give as: Take $\Gamma^0 := \Gamma^h(0) \in \mathbb{X}_p^h$, for $m \geq 0$, find a closed curve $\Gamma^{m+1} := \mathbf{X}^{m+1}(\cdot) = (x^{m+1}(\cdot), y^{m+1}(\cdot))^T \in \mathbb{X}_p^h$ and a weighted mean curvature $\mu^{m+1}(\cdot) \in \mathbb{K}_p^h$, such that

$$\left(\frac{\mathbf{X}^{m+1} - \mathbf{X}^m}{\tau}, \varphi^h \mathbf{n}^m \right)_{\Gamma^m}^h + \left(\partial_s \mu^{m+1}, \partial_s \varphi^h \right)_{\Gamma^m}^h = 0, \quad \forall \varphi^h \in \mathbb{K}_p^h, \quad (4.4a)$$

$$\left(\mu^{m+1}, \mathbf{n}^m \cdot \boldsymbol{\omega}^h \right)_{\Gamma^m}^h - \left(G(\theta^m) \partial_s \mathbf{X}^{m+1}, \partial_s \boldsymbol{\omega}^h \right)_{\Gamma^m}^h = 0, \quad \forall \boldsymbol{\omega}^h \in \mathbb{X}_p^h. \quad (4.4b)$$

The above ES-PFEM is semi-implicit, i.e. only a linear system needs to be solved at each time step, and thus it is very efficient.

4.2. Well-posedness

Assume $N \geq 3$ and denote

$$\tilde{\mathbf{h}}_{N-1}^m := \mathbf{X}^m(\rho_{N-1}) - \mathbf{X}^m(\rho_1), \quad \tilde{\mathbf{h}}_j^m := \mathbf{X}^m(\rho_{j+1}) - \mathbf{X}^m(\rho_{j-1}), \quad j = 1, 2, \dots, N-2, \quad m \geq 0. \quad (4.5)$$

For the well-posedness of the full discretization ES-PFEM (4.4), we have

Theorem 4.1 (Well-posedness). *For each $m \geq 0$, assume that the following two conditions are satisfied*

(i) *at least two vectors in $\{\tilde{\mathbf{h}}_j^m\}_{j=1}^{N-1}$ are not parallel, i.e. there exists $1 \leq j_1 < j_2 \leq N-1$ such that*

$$\tilde{\mathbf{h}}_{j_1}^m \cdot (\tilde{\mathbf{h}}_{j_2}^m)^\perp \neq 0, \quad (4.6)$$

(ii) *no degenerate vertex on Γ^m , i.e.*

$$h_{\min}^m := \min_{1 \leq j \leq N} |\mathbf{h}_j^m| = \min_{1 \leq j \leq N} |\mathbf{X}^m(\rho_{j+1}) - \mathbf{X}^m(\rho_j)| > 0. \quad (4.7)$$

Then the full-discretization (4.4) is well-posed, i.e., there exists a unique solution $(\mathbf{X}^{m+1}, \kappa^{m+1}) \in \mathbb{X}_p^h \times \mathbb{K}_p^h$ of the problem (4.4).

Proof. We just need to prove the following homogeneous problem only has zero solution:

$$\left(\frac{\mathbf{X}^{m+1}}{\tau}, \varphi^h \mathbf{n}^m\right)_{\Gamma^m}^h + \left(\partial_s \mu^{m+1}, \partial_s \varphi^h\right)_{\Gamma^m}^h = 0, \quad \forall \varphi^h \in \mathbb{K}_p^h, \quad (4.8a)$$

$$\left(\mu^{m+1}, \mathbf{n}^m \cdot \boldsymbol{\omega}^h\right)_{\Gamma^m}^h - \left(G(\theta^m) \partial_s \mathbf{X}^{m+1}, \partial_s \boldsymbol{\omega}^h\right)_{\Gamma^m}^h = 0, \quad \forall \boldsymbol{\omega}^h \in \mathbb{X}_p^h. \quad (4.8b)$$

Taking $\varphi^h = \mu^{m+1}$ in (4.8a), we get

$$\left(\frac{\mathbf{X}^{m+1}}{\tau}, \mu^{m+1} \mathbf{n}^m\right)_{\Gamma^m}^h + \left(\partial_s \mu^{m+1}, \partial_s \mu^{m+1}\right)_{\Gamma^m}^h = 0. \quad (4.9)$$

Choosing $\boldsymbol{\omega}^h = \mathbf{X}^{m+1}$ in (4.8b), we have

$$\left(\mu^{m+1}, \mathbf{n}^m \cdot \mathbf{X}^{m+1}\right)_{\Gamma^m}^h - \left(G(\theta^m) \partial_s \mathbf{X}^{m+1}, \partial_s \mathbf{X}^{m+1}\right)_{\Gamma^m}^h = 0. \quad (4.10)$$

Combining (4.9) and (4.10), noting $G(\theta)$ is a positive definite matrix, we obtain

$$\begin{aligned} 0 &\leq \tau \left(\partial_s \mu^{m+1}, \partial_s \mu^{m+1}\right)_{\Gamma^m}^h = - \left(\mathbf{X}^{m+1}, \mu^{m+1} \mathbf{n}^m\right)_{\Gamma^m}^h \\ &= - \left(\mu^{m+1}, \mathbf{n}^m \cdot \mathbf{X}^{m+1}\right)_{\Gamma^m}^h \\ &= - \left(G(\theta^m) \partial_s \mathbf{X}^{m+1}, \partial_s \mathbf{X}^{m+1}\right)_{\Gamma^m}^h \leq 0. \end{aligned} \quad (4.11)$$

Thus we have

$$\left(\partial_s \mu^{m+1}, \partial_s \mu^{m+1}\right)_{\Gamma^m}^h = 0, \quad \left(G(\theta^m) \partial_s \mathbf{X}^{m+1}, \partial_s \mathbf{X}^{m+1}\right)_{\Gamma^m}^h = 0, \quad (4.12)$$

which yields

$$\partial_s \mathbf{X}^{m+1} \equiv \mathbf{0}, \quad \partial_s \mu^{m+1} \equiv 0 \quad \Rightarrow \quad \mathbf{X}^{m+1} \equiv \mathbf{X}^c \in \mathbb{R}^2, \quad \mu^{m+1} \equiv \mu^c \in \mathbb{R}. \quad (4.13)$$

Substituting (4.13) into (4.8), we obtain

$$\left(\frac{\mathbf{X}^c}{\tau}, \varphi^h \mathbf{n}^m\right)_{\Gamma^m}^h = 0, \quad \forall \varphi^h \in \mathbb{K}_p^h, \quad (4.14a)$$

$$\left(\mu^c, \mathbf{n}^m \cdot \boldsymbol{\omega}^h\right)_{\Gamma^m}^h = 0, \quad \forall \boldsymbol{\omega}^h \in \mathbb{X}_p^h. \quad (4.14b)$$

Under the conditions (i) and (ii) and by using the Theorem 2.1 in [6], we know that (4.14) implies $\mu^c = 0$ and $\mathbf{X}^c = \mathbf{0}$. Thus the homogeneous problem (4.8) only has zero solution, and thereby the original inhomogeneous linear system (4.4) is well-posed, i.e. it has a unique solution. \square

4.3. Energy dissipation

Define the total energy W_c^m of the closed curve $\Gamma^m := \mathbf{X}^m$ as

$$W_c^m := W_c(\Gamma^m) = \sum_{j=1}^N |\mathbf{h}_j^m| \gamma(\theta_j^m), \quad m \geq 0. \quad (4.15)$$

We state a generic energy dissipation condition on $\gamma(\theta) \in C^1([-\pi, \pi])$ satisfying $\gamma(-\pi) = \gamma(\pi)$ as

$$2\gamma(\theta) - \gamma(\theta) \cos(\theta - \phi) - \gamma'(\theta) \sin(\theta - \phi) \geq \gamma(\phi), \quad \forall \theta, \phi \in [-\pi, \pi], \quad (4.16)$$

such that the ES-PFEM (4.4) is unconditionally energy stable.

Theorem 4.2 (A generic condition for energy dissipation). *Under the condition (4.16) on $\gamma(\theta)$, the ES-PFEM (4.4) is unconditionally energy stable, i.e. for any $\tau > 0$, we have*

$$W_c^{m+1} \leq W_c^m \leq \dots \leq W_c^0 = \sum_{j=1}^N |\mathbf{h}_j^0| \gamma(\theta_j^0), \quad \forall m \geq 0. \quad (4.17)$$

Proof. Taking $\varphi^h = \mu^{m+1}$ in (4.4a) and $\boldsymbol{\omega}^h = \mathbf{X}^{m+1} - \mathbf{X}^m$ in (4.4b), we get

$$\left(\frac{\mathbf{X}^{m+1} - \mathbf{X}^m}{\tau}, \mu^{m+1} \mathbf{n}^m \right)_{\Gamma^m}^h + \left(\partial_s \mu^{m+1}, \partial_s \mu^{m+1} \right)_{\Gamma^m}^h = 0; \quad (4.18a)$$

$$\left(\mu^{m+1}, \mathbf{n}^m \cdot (\mathbf{X}^{m+1} - \mathbf{X}^m) \right)_{\Gamma^m}^h - \left(G(\theta^m) \partial_s \mathbf{X}^{m+1}, \partial_s \mathbf{X}^{m+1} - \partial_s \mathbf{X}^m \right)_{\Gamma^m}^h = 0. \quad (4.18b)$$

Combining (4.18), (3.4) and (2.11), we have

$$\begin{aligned} & \left(G(\theta^m) \partial_s \mathbf{X}^{m+1}, \partial_s \mathbf{X}^{m+1} - \partial_s \mathbf{X}^m \right)_{\Gamma^m}^h + \int_{\Gamma^m} \gamma(\theta^m) ds \\ &= \sum_{j=1}^N |\mathbf{h}_j^m| \left(\frac{\mathbf{h}_j^{m+1}}{|\mathbf{h}_j^m|} \cdot \frac{\mathbf{h}_j^{m+1} - \mathbf{h}_j^m}{|\mathbf{h}_j^m|} \right) \gamma(\theta_j^m) + \sum_{j=1}^N |\mathbf{h}_j^m| \left(\frac{(\mathbf{h}_j^{m+1})^\perp}{|\mathbf{h}_j^{m+1}|} \cdot \frac{\mathbf{h}_j^m}{|\mathbf{h}_j^m|} \right) \gamma'(\theta_j^m) + \sum_{j=1}^N |\mathbf{h}_j^m| \gamma(\theta_j^m) \\ &= \sum_{j=1}^N |\mathbf{h}_j^m| \left(\frac{|\mathbf{h}_j^{m+1}| \boldsymbol{\tau}_j^{m+1}}{|\mathbf{h}_j^m|} \cdot \frac{|\mathbf{h}_j^{m+1}| \boldsymbol{\tau}_j^{m+1} - |\mathbf{h}_j^m| \boldsymbol{\tau}_j^m}{|\mathbf{h}_j^m|} \right) \gamma(\theta_j^m) \\ &\quad + \sum_{j=1}^N |\mathbf{h}_j^m| \left(\frac{|\mathbf{h}_j^{m+1}| (\boldsymbol{\tau}_j^{m+1})^\perp}{|\mathbf{h}_j^m|} \cdot \frac{|\mathbf{h}_j^m| \boldsymbol{\tau}_j^m}{|\mathbf{h}_j^m|} \right) \gamma'(\theta_j^m) + \sum_{j=1}^N |\mathbf{h}_j^m| \gamma(\theta_j^m) \\ &= \sum_{j=1}^N \frac{|\mathbf{h}_j^{m+1}|^2 \gamma(\theta_j^m) + |\mathbf{h}_j^{m+1}| |\mathbf{h}_j^m| [\gamma'(\theta_j^m) \sin(\theta_j^{m+1} - \theta_j^m) - \gamma(\theta_j^m) \cos(\theta_j^{m+1} - \theta_j^m)] + |\mathbf{h}_j^m|^2 \gamma(\theta_j^m)}{|\mathbf{h}_j^m|}, \end{aligned} \quad (4.19)$$

where

$$\boldsymbol{\tau}_j^{m+1} = (\cos \theta_j^{m+1}, \sin \theta_j^{m+1})^T, \quad \boldsymbol{\tau}_j^m = (\cos \theta_j^m, \sin \theta_j^m)^T, \quad j = 1, 2, \dots, N.$$

By the inequality of arithmetic and geometric means, we have

$$|\mathbf{h}_j^{m+1}|^2 \gamma(\theta_j^m) + |\mathbf{h}_j^m|^2 \gamma(\theta_j^m) \geq 2 |\mathbf{h}_j^m| |\mathbf{h}_j^{m+1}| \gamma(\theta_j^m), \quad j = 1, 2, \dots, N, \quad m \geq 0. \quad (4.20)$$

Combining (4.16), (4.20) and (4.19), we get

$$\begin{aligned} & \left(G(\theta^m) \partial_s \mathbf{X}^{m+1}, \partial_s \mathbf{X}^{m+1} - \partial_s \mathbf{X}^m \right)_{\Gamma^m}^h + \int_{\Gamma^m} \gamma(\theta^m) ds \\ &\geq \sum_{j=1}^N \frac{|\mathbf{h}_j^{m+1}| |\mathbf{h}_j^m| [2\gamma(\theta_j^m) - \gamma(\theta_j^m) \cos(\theta_j^{m+1} - \theta_j^m) + \gamma'(\theta_j^m) \sin(\theta_j^{m+1} - \theta_j^m)]}{|\mathbf{h}_j^m|} \\ &= \sum_{j=1}^N |\mathbf{h}_j^{m+1}| [2\gamma(\theta_j^m) - \gamma(\theta_j^m) \cos(\theta_j^m - \theta_j^{m+1}) - \gamma'(\theta_j^m) \sin(\theta_j^m - \theta_j^{m+1})] \\ &\geq \sum_{j=1}^N |\mathbf{h}_j^{m+1}| \gamma(\theta_j^{m+1}) = \int_{\Gamma^{m+1}} \gamma(\theta_j^{m+1}) ds. \end{aligned} \quad (4.21)$$

Combining the final result in (4.21), (4.18a) and (4.18b), we have,

$$\begin{aligned}
W_c^{m+1} - W_c^m &= \int_{\Gamma^{m+1}} \gamma(\theta^{m+1}) ds - \int_{\Gamma^m} \gamma(\theta^m) ds \\
&\leq \left(G(\theta^m) \partial_s \mathbf{X}^{m+1}, \partial_s \mathbf{X}^{m+1} - \partial_s \mathbf{X}^m \right)_{\Gamma^m}^h + \int_{\Gamma^m} \gamma(\theta^m) ds - \int_{\Gamma^m} \gamma(\theta^m) ds \\
&= \left(G(\theta^m) \partial_s \mathbf{X}^{m+1}, \partial_s \mathbf{X}^{m+1} - \partial_s \mathbf{X}^m \right)_{\Gamma^m}^h \\
&= \left(\mu^{m+1}, \mathbf{n}^m \cdot (\mathbf{X}^{m+1} - \mathbf{X}^m) \right)_{\Gamma^m}^h \\
&= -\tau \left(\partial_s \mu^{m+1}, \partial_s \mu^{m+1} \right)_{\Gamma^m}^h \leq 0, \quad m \geq 0,
\end{aligned} \tag{4.22}$$

which immediately implies the energy dissipation in (4.17). \square

From the linearity and translation invariance with respect to $\gamma(\theta)$ in the energy dissipation condition (4.16), we have

Corollary 4.1 (Addition, scalar multiplication and translation). *Assume that $\gamma_1(\theta)$, $\gamma_2(\theta)$ be two anisotropic surface energies satisfying the energy dissipation condition (4.16), θ_0 is a given constant. Then $\gamma(\theta) = c\gamma_1(\theta)$ with $c > 0$, $\gamma(\theta) = \gamma_1(\theta) + \gamma_2(\theta)$ and $\gamma(\theta) = \gamma_1(\theta - \theta_0)$ also satisfy the energy dissipation condition (4.16).*

Now we apply the result in Theorem 4.2 to the ellipsoidal anisotropy surface energy (1.7) and obtain a simple energy dissipation condition in this special case.

Corollary 4.2 (Ellipsoidal anisotropic surface energy). *For the ellipsoidal anisotropic surface energy $\gamma(\theta)$ in (1.7), assume $-a/2 \leq b \leq a$, then it satisfies the energy dissipation condition (4.16), and thus the ES-PFEM (4.4) is unconditionally energy stable.*

Proof. Noticing that $\gamma(\theta) = \sqrt{a + b \cos^2 \theta} = \sqrt{a} \sqrt{1 + \beta \cos^2 \theta}$ with $\beta := \frac{b}{a}$ and by Corollary 4.1, we need only to prove the case when $a = 1$ and $-1/2 \leq b = \beta \leq 1$. Then we have

$$\begin{aligned}
&2\gamma(\theta) - \gamma(\theta) \cos(\theta - \phi) - \gamma'(\theta) \sin(\theta - \phi) - \gamma(\phi) \\
&= \frac{(2 - \cos(\theta - \phi))\gamma^2(\theta) + \beta \cos(\theta) \sin(\theta) \sin(\theta - \phi) - \gamma(\theta)\gamma(\phi)}{\gamma(\theta)} \\
&\geq \frac{1}{\gamma(\theta)} \left((2 - \cos(\theta - \phi))\gamma^2(\theta) + \beta \cos(\theta) \sin(\theta) \sin(\theta - \phi) - \frac{\gamma^2(\theta) + \gamma^2(\phi)}{2} \right) \\
&= \frac{1}{\gamma(\theta)} \sin^2 \left(\frac{\theta - \phi}{2} \right) (\beta \cos(\theta + \phi) + 2\beta \cos(2\theta) + \beta + 2) \\
&\geq \frac{1}{\gamma(\theta)} \sin^2 \left(\frac{\theta - \phi}{2} \right) \min\{2 - 2\beta, 2 + 4\beta\} \geq 0, \quad \forall \theta, \phi \in [-\pi, \pi],
\end{aligned}$$

which immediately implies $\gamma(\theta)$ satisfies the energy dissipation condition (4.16). \square

Corollary 4.3 (Riemannian metric anisotropic surface energy). *For the Riemannian metric anisotropic surface energy $\gamma(\theta)$ in (1.8), assume $0 < \lambda_k^{(1)} \leq \lambda_k^{(2)}$ be the two eigenvalues of the symmetric positive definite matrix G_k for $k = 1, 2, \dots, K$. If $\lambda_k^{(2)} \leq 2\lambda_k^{(1)}$ for $k = 1, 2, \dots, K$, then $\gamma(\theta)$ satisfies the energy dissipation condition (4.16), and thus the ES-PFEM (4.4) is unconditionally energy stable.*

Proof. By Corollary 4.1, it suffices that we prove it is true when $K = 1$. When $K = 1$ in (1.8), since G_1 is a symmetric positive definite matrix, thus there exists an orthonormal matrix (or a rotation matrix) $R_1 \in \mathbb{R}^{2 \times 2}$ such that

$$R_1 = \begin{pmatrix} \cos \theta_1 & -\sin \theta_1 \\ \sin \theta_1 & \cos \theta_1 \end{pmatrix}, \quad R_1^T G_1 R_1 = \begin{pmatrix} \lambda_1^{(1)} & 0 \\ 0 & \lambda_1^{(2)} \end{pmatrix}, \quad \mathbf{n}(\theta) = R_1 \mathbf{n}(\theta - \theta_1), \tag{4.23}$$

where $\theta_1 \in [-\pi, \pi]$ is a constant, $0 < \lambda_1^{(1)} \leq \lambda_1^{(2)}$ are the two eigenvalues of G_1 , and $\mathbf{n}(\theta)$ is given in (1.8). Plugging (4.23) into (1.8) with $K = 1$, we get

$$\gamma(\theta) = \sqrt{\mathbf{n}(\theta)^T G_1 \mathbf{n}(\theta)} = \sqrt{(\mathbf{n}(\theta - \theta_1))^T (R_1^T G_1 R_1) \mathbf{n}(\theta - \theta_1)} = \sqrt{\lambda_1^{(1)} + (\lambda_1^{(2)} - \lambda_1^{(1)}) \cos^2(\theta - \theta_1)}. \quad (4.24)$$

It is easy to see that $\lambda_1^{(2)} - \lambda_1^{(1)} \geq 0 \geq -\frac{1}{2}\lambda_1^{(1)}$. Thus by Corollaries 4.2 and 4.1, when $\lambda_1^{(2)} - \lambda_1^{(1)} \leq \lambda_1^{(1)}$, i.e. $\lambda_1^{(2)} \leq 2\lambda_1^{(1)}$, then $\gamma(\theta)$ satisfies the energy dissipation condition (4.16). \square

Assume

$$\gamma(\theta) = \frac{a_0}{2} + \sum_{l=1}^{\infty} [a_l \cos(l\theta) + b_l \sin(l\theta)], \quad -\pi \leq \theta \leq \pi, \quad (4.25)$$

where a_l ($l \geq 0$) and b_l ($l \geq 1$) are the Fourier coefficients of $\gamma(\theta)$, which are given as

$$a_l = \frac{1}{\pi} \int_{-\pi}^{\pi} \gamma(\theta) \cos(l\theta) d\theta, \quad b_l = \frac{1}{\pi} \int_{-\pi}^{\pi} \gamma(\theta) \sin(l\theta) d\theta, \quad l \geq 0. \quad (4.26)$$

Then we can state a specific energy dissipation condition on $\gamma(\theta)$, which can be easily applied to the k -fold anisotropy surface energy (1.6).

Theorem 4.3 (A specific condition for energy dissipation). *Assume*

$$\frac{a_0}{2} \geq \sum_{l=1}^{\infty} (1 + l^2) \sqrt{a_l^2 + b_l^2}, \quad (4.27)$$

then the anisotropic surface energy $\gamma(\theta)$ satisfies the energy dissipation condition (4.16), and thus the ES-PFEM (4.4) is unconditionally energy stable.

Proof. Under the assumption (4.27), we have

$$\gamma'(\theta) = \sum_{l=1}^{\infty} l [-a_l \sin(l\theta) + b_l \cos(l\theta)], \quad \theta \in [-\pi, \pi]. \quad (4.28)$$

Plugging (4.26) and (4.28) into (4.16), we get

$$\begin{aligned} & 2\gamma(\theta) - \gamma(\theta) \cos(\theta - \phi) - \gamma(\phi) - \gamma'(\theta) \sin(\theta - \phi) \\ &= \gamma(\theta)(1 - \cos(\theta - \phi)) + \gamma(\theta) - \gamma(\phi) - \gamma'(\theta) \sin(\theta - \phi) \\ &= \gamma(\theta)(1 - \cos(\theta - \phi)) + \sum_{l=1}^{\infty} \left[a_l [\cos(l\theta) - \cos(l\phi) + l \sin(l\theta) \sin(\theta - \phi)] \right. \\ & \quad \left. + b_l [\sin(l\theta) - \sin(l\phi) - l \cos(l\theta) \sin(\theta - \phi)] \right]. \end{aligned}$$

By Lemma B.1 in Appendix B, noting (4.27), we have

$$\begin{aligned} & 2\gamma(\theta) - \gamma(\theta) \cos(\theta - \phi) - \gamma(\phi) - \gamma'(\theta) \sin(\theta - \phi) \\ & \geq \gamma(\theta)(1 - \cos(\theta - \phi)) - \sum_{l=1}^{\infty} \left((1 - \cos(\theta - \phi)) l^2 \sqrt{a_l^2 + b_l^2} \right) \\ &= (1 - \cos(\theta - \phi)) \left(\frac{a_0}{2} + \sum_{l=1}^{\infty} \left(a_l \cos(l\theta) + b_l \sin(l\theta) - l^2 \sqrt{a_l^2 + b_l^2} \right) \right) \\ & \geq (1 - \cos(\theta - \phi)) \left(\frac{a_0}{2} - \sum_{l=1}^{\infty} (1 + l^2) \sqrt{a_l^2 + b_l^2} \right) \\ & \geq 0, \quad \forall \theta, \phi \in [-\pi, \pi], \end{aligned} \quad (4.29)$$

which immediately implies $\gamma(\theta)$ satisfies the energy dissipation condition (4.16). \square

By using Theorem 4.3, we can find a sufficient condition on the k -fold anisotropy energy $\gamma(\theta)$ in (1.6) so that it satisfies the energy dissipation condition (4.16). Furthermore, we can prove that the condition is also necessary in this special case, which implies that our Theorem 4.3 is sharp and can hardly be improved.

Corollary 4.4 (k -fold anisotropic surface energy). *For the k -fold anisotropy energy $\gamma(\theta)$ in (1.6), it satisfies the energy dissipation condition (4.16) if and only if*

$$|\beta| \leq \beta_{\max} := \frac{1}{1+k^2}. \quad (4.30)$$

Proof. (\Leftarrow) Combining (1.6) and (4.25), we have

$$a_0 = 2, \quad a_k = \beta \cos(k\theta_0), \quad b_k = \beta \sin(k\theta_0), \quad a_l = b_l = 0, \quad 1 \leq l \neq k. \quad (4.31)$$

Combining (4.31) and (4.27), under the condition (4.30), we obtain

$$\sum_{l=1}^{\infty} (1+l^2) \sqrt{a_l^2 + b_l^2} = (1+k^2) \sqrt{a_k^2 + b_k^2} = (1+k^2) |\beta| \leq (1+k^2) \frac{1}{1+k^2} = 1 = \frac{a_0}{2}, \quad (4.32)$$

which implies that (4.27) is satisfied and thus the energy dissipation condition (4.16) is satisfied.

(\Rightarrow) Denote

$$g(\phi) = 2\gamma(\theta) - \gamma(\theta) \cos(\theta - \phi) - \gamma'(\theta) \sin(\theta - \phi) - \gamma(\phi), \quad \phi \in [-\pi, \pi]. \quad (4.33)$$

Differentiating (4.33) with respect to ϕ , we have

$$g'(\phi) = -\gamma(\theta) \sin(\theta - \phi) + \gamma'(\theta) \cos(\theta - \phi) - \gamma'(\phi), \quad (4.34a)$$

$$g''(\phi) = \gamma(\theta) \cos(\theta - \phi) + \gamma'(\theta) \sin(\theta - \phi) - \gamma''(\phi). \quad (4.34b)$$

Taking $\phi = \theta$ in (4.33) and (4.34), we obtain

$$g(\theta) = g'(\theta) = 0, \quad g''(\theta) = \gamma(\theta) - \gamma''(\theta), \quad \theta \in [-\pi, \pi]. \quad (4.35)$$

The energy dissipation (4.16) implies

$$g(\phi) \geq 0, \quad \forall \theta, \phi \in [-\pi, \pi]. \quad (4.36)$$

Combining (4.36) and (4.35), noticing (1.6), we have

$$0 \leq g''(\phi)|_{\phi=\theta} = g''(\theta) = \gamma(\theta) - \gamma''(\theta) = 1 + (1+k^2)\beta \cos(k(\theta - \theta_0)), \quad \forall \theta \in [-\pi, \pi], \quad (4.37)$$

which immediately implies the condition (4.30). \square

If $\gamma(\theta) \in C^3([-\pi, \pi])$, we can state another specific energy dissipation condition on $\gamma(\theta)$.

Theorem 4.4 (Another specific condition for energy dissipation). *If $\gamma(\theta) \in C^3([-\pi, \pi])$ satisfies*

$$\int_{-\pi}^{\pi} \frac{\gamma(\theta)}{2\pi} d\theta \geq \frac{5}{2} \left\| \gamma^{(3)}(\theta) \right\|_{L^2}, \quad (4.38)$$

then it satisfies the energy dissipation condition (4.16), and thus the ES-PFEM (4.4) is unconditionally energy stable.

Proof. Plugging (4.25) into the left-hand of (4.38), we get

$$\int_{-\pi}^{\pi} \frac{\gamma(\theta)}{2\pi} d\theta = \frac{a_0}{2}. \quad (4.39)$$

Similarly, plugging (4.25) into the right-hand of (4.38) and applying the Cauchy-Schwarz inequality, we get

$$\begin{aligned} \|\gamma^{(3)}(\theta)\|_{L^2} &= \left(\sum_{l=1}^{\infty} l^6 (a_l^2 + b_l^2) \right)^{1/2} \\ &= \left(\sum_{l=1}^{\infty} \frac{(1+l^2)^2}{l^6} \right)^{-1/2} \left[\left(\sum_{l=1}^{\infty} l^6 (a_l^2 + b_l^2) \right)^{1/2} \left(\sum_{l=1}^{\infty} \frac{(1+l^2)^2}{l^6} \right)^{1/2} \right] \\ &\geq \left(\sum_{l=1}^{\infty} \frac{(1+l^2)^2}{l^6} \right)^{-1/2} \left(\sum_{l=1}^{\infty} (1+l^2) \sqrt{a_l^2 + b_l^2} \right). \end{aligned} \quad (4.40)$$

By using Fourier series, we have the following estimate

$$\sum_{l=1}^{\infty} \frac{(1+l^2)^2}{l^6} = \frac{2\pi^4 + 42\pi^3 + 315\pi^2}{1890} \leq \frac{25}{4} \quad \Rightarrow \quad \left(\sum_{l=1}^{\infty} \frac{(1+l^2)^2}{l^6} \right)^{-1/2} \geq \frac{2}{5}. \quad (4.41)$$

Combining (4.39), (4.40) and (4.41), we obtain

$$\frac{a_0}{2} = \int_{-\pi}^{\pi} \frac{\gamma(\theta)}{2\pi} d\theta \geq \frac{5}{2} \|\gamma^{(3)}(\theta)\|_{L^2} \geq \sum_{l=1}^{\infty} (1+l^2) \sqrt{a_l^2 + b_l^2}, \quad (4.42)$$

which immediately implies (4.27) is satisfied, and thus (4.16) is satisfied by using Theorem 4.3. \square

5. Extension to solid-state dewetting

In this section, we extend the new and simple variational formulation (2.16) and its ES-PFEM (4.4) for a closed curve under anisotropic surface diffusion to solid-state dewetting in materials science [3, 19, 29], i.e. evolution of an open curve under anisotropic surface diffusion and contact line migration (cf. Figure 2).

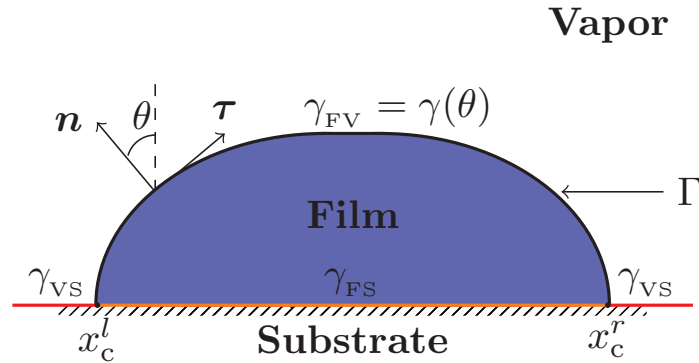


Figure 2: A schematic illustration of a thin film on a rigid, flat substrate (i.e., the x -axis) in two dimensions, where x_c^l and x_c^r are the left and right contact points, $\gamma_{FV} = \gamma(\theta)$, γ_{VS} and γ_{FS} represent the film vapor, vapor substrate and film substrate surface energy densities, respectively.

5.1. A sharp interface model and its new variational formulation

As shown in Figure 2, a typical problem in solid-state dewetting is to study the motion of an open curve $\Gamma := \Gamma(t)$ under anisotropic surface diffusion with its two contact points $x_c^l := x_c^l(t)$ and $x_c^r := x_c^r(t)$ moving along the rigid flat substrate. By adapting the same notations in the previous sections except removing the periodic boundary conditions, we represent $\Gamma(t) := \mathbf{X}(\rho, t) = (x(\rho, t), y(\rho, t))^T$ for $0 \leq \rho \leq 1$ (or respectively, $\Gamma(t) := \mathbf{X}(s, t) = (x(s, t), y(s, t))^T$ with $0 \leq s \leq L(t)$ the arc length parameter and $L(t)$ the length of $\Gamma(t)$). As it was derived in the literature [3, 19, 29], $\mathbf{X}(\rho, t)$ satisfies the anisotropic surface diffusion (1.1)-(1.2) and the following boundary conditions: [3, 19, 29]

(i) contact point condition

$$y(0, t) = 0, \quad y(1, t) = 0, \quad t \geq 0; \quad (5.1)$$

(ii) relaxed contact angle condition

$$\frac{dx_c^l(t)}{dt} = \eta f(\theta_d^l; \sigma), \quad \frac{dx_c^r(t)}{dt} = -\eta f(\theta_d^r; \sigma), \quad t \geq 0; \quad (5.2)$$

(iii) zero-mass flux condition

$$\partial_s \mu(0, t) = 0, \quad \partial_s \mu(1, t) = 0, \quad t \geq 0; \quad (5.3)$$

satisfying $x_c^l(t) = x(0, t) \leq x_c^r(t) = x(1, t)$, where $\theta_d^l := \theta_d^l(t)$ and $\theta_d^r := \theta_d^r(t)$ are the contact angles at the left and the right contact points, respectively. $0 < \eta < \infty$ denotes the contact line mobility and $f(\theta; \sigma)$ is defined as

$$f(\theta; \sigma) = \gamma(\theta) \cos \theta - \gamma'(\theta) \sin \theta - \sigma, \quad \theta \in [-\pi, \pi], \quad (5.4)$$

with $\sigma = \cos \theta_i = \frac{\gamma_{VS} - \gamma_{FS}}{\gamma_0}$ and θ_i and γ_0 being the isotropic Young contact angle and dimensionless surface energy unit, respectively [3, 19, 29]. The initial condition is given as (1.3) satisfying $y_0(0) = y_0(L_0) = 0$ and $x_c^l(0) = x_0(0) \leq x_c^r(0) = x_0(L_0)$ with L_0 the length of the curve at $t = 0$.

Let $A(t)$ (defined in (1.9)) be the area/mass of the region enclosed by $\Gamma(t)$ and the flat substrate, and define the total interfacial energy $W_o(t)$ as

$$W_o(t) = \int_{\Gamma(t)} \gamma(\theta) ds - \sigma(x_c^r(t) - x_c^l(t)), \quad t \geq 0. \quad (5.5)$$

As it was proven in the literature [3, 19, 29], we have [3]

$$\frac{d}{dt} A(t) = 0, \quad \frac{d}{dt} W_o(t) = - \int_{\Gamma(t)} |\partial_s \mu|^2 ds - \frac{1}{\eta} \left[\left(\frac{dx_c^r(t)}{dt} \right)^2 + \left(\frac{dx_c^l(t)}{dt} \right)^2 \right] \leq 0, \quad t \geq 0, \quad (5.6)$$

which implies area/mass conservation and energy dissipation, i.e.

$$A(t) \equiv A(0), \quad W_o(t) \leq W_o(t_1) \leq W_o(0) = \int_{\Gamma(0)} \gamma(\theta) ds - \sigma(x_c^r(0) - x_c^l(0)), \quad t \geq t_1 \geq 0. \quad (5.7)$$

Introduce the functional spaces

$$H_0^1(\mathbb{I}) := \{u \in H^1(\mathbb{I}) \mid u(0) = u(1) = 0\}, \quad \mathbb{X} := H^1(\mathbb{I}) \times H_0^1(\mathbb{I}). \quad (5.8)$$

Similar to those derivations in Section 2, we can obtain a new and simple variational formulation for (2.1) with the boundary conditions (5.1)-(5.3) and the initial condition (1.3) as: Given an initial open curve $\Gamma(0) := \mathbf{X}(\cdot, 0) = \mathbf{X}_0 \in \mathbb{X}$, find an open curve $\Gamma(t) = \mathbf{X}(\cdot, t) \in \mathbb{X}$ and $\mu(t) \in \mathbb{K}$, such that:

$$\left(\partial_t \mathbf{X}, \varphi \mathbf{n} \right)_{\Gamma(t)} + \left(\partial_s \mu, \partial_s \varphi \right)_{\Gamma(t)} = 0, \quad \forall \varphi \in \mathbb{K}, \quad (5.9a)$$

$$\begin{aligned} \left(\mu, \mathbf{n} \cdot \boldsymbol{\omega} \right)_{\Gamma(t)} - \left(G(\theta) \partial_s \mathbf{X}, \partial_s \boldsymbol{\omega} \right)_{\Gamma(t)} - \frac{1}{\eta} \left[\frac{dx_c^l(t)}{dt} \omega_1(0) + \frac{dx_c^r(t)}{dt} \omega_1(1) \right] \\ + \sigma [\omega_1(1) - \omega_1(0)] = 0, \quad \forall \boldsymbol{\omega} = (\omega_1, \omega_2)^T \in \mathbb{X}, \end{aligned} \quad (5.9b)$$

satisfying $x_c^l(t) = x(0, t) \leq x_c^r(t) = x(1, t)$.

Similar to the closed curve case, one can easily show area/mass conservation and energy dissipation of the variational problem (5.9), i.e. (5.7) is valid. The details are omitted here for brevity.

5.2. An energy-stable PFEM and its properties

Introduce the finite element subspaces

$$\mathbb{K}_0^h := \{u^h \in \mathbb{K}^h \mid u^h(0) = u^h(1) = 0\}, \quad \mathbb{X}^h := \mathbb{K}^h \times \mathbb{K}_0^h. \quad (5.10)$$

Similar to Section 3, we can discretize (5.9) in space by PFEM and establish its area/mass conservation and energy dissipation of the semi-discretization. Again, the details are omitted here for brevity.

For each $m \geq 0$, let $\Gamma^m := \mathbf{X}^m(\rho) = (x^m(\rho), y^m(\rho))^T \in \mathbb{X}^h$ and $\mu^m \in \mathbb{K}^h$ be the approximations of $\Gamma(\cdot, t_m) = \mathbf{X}(\rho, t_m) \in \mathbb{X}$ and $\mu(\cdot, t_m) \in \mathbb{K}$, respectively, which is the solution of the variational problem (5.9) with the initial data (1.3). Let $\Gamma^0 := \mathbf{X}^0(\rho) = (x^0(\rho), y^0(\rho))^T \in \mathbb{X}^h$ be an interpolation of the initial curve $\mathbf{X}_0(s)$ in (1.3), which is defined as $\mathbf{X}^0(\rho = \rho_j) = \mathbf{X}_0(s = s_j^0)$ with $s_j^0 = L_0 \rho_j$ for $j = 0, 1, \dots, N$. Then an energy-stable PFEM (**ES-PFEM**) for discretizing (5.9) with (1.3) is given as: Take $\Gamma^0 = \mathbf{X}^0(\cdot) \in \mathbb{X}^h$ satisfying $x^0(0) \leq x^0(1)$ and $y^0(0) = y^0(1) = 0$, and set $x_l^0 := x^0(0)$ and $x_r^0 := x^0(1)$, for $m \geq 0$, find $\Gamma^{m+1} = \mathbf{X}^{m+1}(\cdot) = (x^{m+1}(\cdot), y^{m+1}(\cdot))^T \in \mathbb{X}^h$ and $\mu^{m+1}(\cdot) \in \mathbb{K}^h$, such that

$$\left(\frac{\mathbf{X}^{m+1} - \mathbf{X}^m}{\tau}, \varphi^h \mathbf{n}^m \right)_{\Gamma^m}^h + \left(\partial_s \mu^{m+1}, \partial_s \varphi^h \right)_{\Gamma^m}^h = 0, \quad \forall \varphi^h \in \mathbb{K}^h, \quad (5.11a)$$

$$\begin{aligned} & \left(\mu^{m+1}, \mathbf{n}^m \cdot \boldsymbol{\omega}^h \right)_{\Gamma^m}^h - \left(G(\theta^m) \partial_s \mathbf{X}^{m+1}, \partial_s \boldsymbol{\omega}^h \right)_{\Gamma^m}^h - \frac{1}{\eta} \left[\frac{x_l^{m+1} - x_l^m}{\tau} \omega_1^h(0) + \frac{x_r^{m+1} - x_r^m}{\tau} \omega_1^h(1) \right] \\ & + \sigma \left[\omega_1^h(1) - \omega_1^h(0) \right] = 0, \quad \forall \boldsymbol{\omega}^h \in \mathbb{X}^h, \end{aligned} \quad (5.11b)$$

satisfying $x_l^{m+1} = x^{m+1}(0) \leq x_r^{m+1} = x^{m+1}(1)$.

The above ES-PFEM is semi-implicit, i.e. only a linear system needs to be solved at each time step, and thus it is very efficient. We have the following result for its well-posedness.

Theorem 5.1 (Well-posedness). *For each $m \geq 0$, assume the condition (4.7) is valid and at least one of \mathbf{h}_1^m and \mathbf{h}_N^m is not horizontal, i.e.*

$$(\mathbf{h}_1^m \cdot \mathbf{e}_2)^2 + (\mathbf{h}_N^m \cdot \mathbf{e}_2)^2 > 0, \quad \text{with } \mathbf{e}_2 = (0, 1)^T. \quad (5.12)$$

Then the full-discretization (5.11) is well-posed, i.e., there exists a unique solution $(\mathbf{X}^{m+1}, \kappa^{m+1}) \in (\mathbb{X}^h, \mathbb{K}^h)$.

Proof. Again, we just need to prove the following homogeneous problem only has zero solution:

$$\left(\frac{\mathbf{X}^{m+1}}{\tau}, \varphi^h \mathbf{n}^m \right)_{\Gamma^m}^h + \left(\partial_s \mu^{m+1}, \partial_s \varphi^h \right)_{\Gamma^m}^h = 0, \quad \forall \varphi^h \in \mathbb{K}^h, \quad (5.13a)$$

$$\left(\mu^{m+1}, \mathbf{n}^m \cdot \boldsymbol{\omega}^h \right)_{\Gamma^m}^h - \left(G(\theta^m) \partial_s \mathbf{X}^{m+1}, \partial_s \boldsymbol{\omega}^h \right)_{\Gamma^m}^h - \frac{x_l^{m+1} \omega_1^h(0) + x_r^{m+1} \omega_1^h(1)}{\eta \tau} = 0, \quad \forall \boldsymbol{\omega}^h \in \mathbb{X}^h. \quad (5.13b)$$

Taking $\varphi^h = \mu^{m+1}$ in (5.13a) and $\boldsymbol{\omega}^h = \mathbf{X}^{m+1}$ in (5.13b), multiplying the first one by τ , and then subtracting it by the second one, we obtain

$$\tau \left(\partial_s \mu^{m+1}, \partial_s \mu^{m+1} \right)_{\Gamma^m}^h + \left(\gamma(\theta^m) \partial_s \mathbf{X}^{m+1}, \partial_s \mathbf{X}^{m+1} \right)_{\Gamma^m}^h + \frac{(x_l^{m+1})^2 + (x_r^{m+1})^2}{\eta \tau} = 0. \quad (5.14)$$

Since $G(\theta)$ is a positive definite matrix and thus the left hand side of (5.14) is the summation of squares, we obtain

$$\partial_s \mathbf{X}^{m+1} \equiv \mathbf{0}, \quad \partial_s \mu^{m+1} \equiv 0, \quad x_l^{m+1} = 0, \quad x_r^{m+1} = 0. \quad (5.15)$$

This, together with $\mathbf{X}^{m+1} \in \mathbb{X}^h$ and $\mu^{m+1} \in \mathbb{K}^h$, implies that

$$\mathbf{X}^{m+1} \equiv \mathbf{0}, \quad \mu^{m+1} \equiv \mu^c \in \mathbb{R}. \quad (5.16)$$

Substituting (5.16) into (5.13b), we obtain

$$\left(\mu^c, \mathbf{n}^m \cdot \boldsymbol{\omega}^h \right)_{\Gamma^m}^h = 0, \quad \forall \boldsymbol{\omega}^h = (\omega_1^h, \omega_2^h)^T \in \mathbb{X}^h. \quad (5.17)$$

Under the assumptions (4.7) and (5.12) and by using Theorem 4.1 in [31], then (5.17) implies $\mu^c = 0$. Thus the homogeneous problem (5.13) only has zero solution, and thereby the original inhomogeneous linear system (5.11) is well-posed. \square

Define the total interfacial energy of the open polygonal curve Γ^m as

$$W_o^m := W_o(\Gamma^m) = \sum_{j=1}^N |\mathbf{h}_j^m| \gamma(\theta_j^m) - \sigma(x_r^m - x_l^m), \quad m \geq 0. \quad (5.18)$$

Then for the ES-PFEM (5.11), we have the following results on its energy dissipation.

Theorem 5.2 (Energy dissipation). *Under the condition (4.16) on $\gamma(\theta)$, the ES-PFEM (5.11) is unconditionally energy-stable, i.e. for any $\tau > 0$, we have*

$$W_o^{m+1} \leq W_o^m \leq \dots \leq W_o^0 := \sum_{j=1}^N |\mathbf{h}_j^0| \gamma(\theta_j^0) - \sigma(x_r^0 - x_l^0), \quad \forall m \geq 0. \quad (5.19)$$

Proof. Taking $\varphi^h = \mu^{m+1}$ in (5.11a) and $\boldsymbol{\omega}^h = \mathbf{X}^{m+1} - \mathbf{X}^m$ in (5.11b), multiplying the first one by τ , and then subtracting it by the second one, we obtain

$$\begin{aligned} & \tau \left(\partial_s \mu^{m+1}, \partial_s \mu^{m+1} \right)_{\Gamma^m}^h + \left(G(\theta^m) \partial_s \mathbf{X}^{m+1}, \partial_s \mathbf{X}^{m+1} - \partial_s \mathbf{X}^m \right)_{\Gamma^m}^h \\ & + \frac{1}{\eta} \left[\frac{(x_l^{m+1} - x_r^m)^2}{\tau} + \frac{(x_r^{m+1} - x_l^m)^2}{\tau} \right] - \sigma \left[(x_r^{m+1} - x_r^m) - (x_l^{m+1} - x_l^m) \right] = 0. \end{aligned} \quad (5.20)$$

Under the condition (4.16) and noting (4.21), we get

$$\begin{aligned} W_o^{m+1} - W_o^m &= \int_{\Gamma^{m+1}} \gamma(\mathbf{n}^{m+1}) ds - \sigma(x_r^{m+1} - x_l^{m+1}) - \int_{\Gamma^m} \gamma(\mathbf{n}^m) ds + \sigma(x_r^m - x_l^m) \\ &\leq \left(G(\theta^m) \partial_s \mathbf{X}^{m+1}, \partial_s \mathbf{X}^{m+1} - \partial_s \mathbf{X}^m \right)_{\Gamma^m}^h + \int_{\Gamma^m} \gamma(\mathbf{n}^m) ds \\ &\quad - \sigma(x_r^{m+1} - x_l^{m+1}) - \int_{\Gamma^m} \gamma(\mathbf{n}^m) ds + \sigma(x_r^m - x_l^m) \\ &= \left(G(\theta^m) \partial_s \mathbf{X}^{m+1}, \partial_s \mathbf{X}^{m+1} - \partial_s \mathbf{X}^m \right)_{\Gamma^m}^h - \sigma \left[(x_r^{m+1} - x_r^m) - (x_l^{m+1} - x_l^m) \right] \\ &= -\tau \left(\partial_s \mu^{m+1}, \partial_s \mu^{m+1} \right)_{\Gamma^m}^h - \frac{1}{\eta} \left[\frac{(x_l^{m+1} - x_l^m)^2}{\tau} + \frac{(x_r^{m+1} - x_r^m)^2}{\tau} \right] \\ &\leq 0, \quad m \geq 0, \end{aligned} \quad (5.21)$$

which immediately implies the energy dissipation (5.19). \square

Remark 5.1. *All the results in Section 4 on energy dissipation of the ES-PFEM (4.4) for motion of a closed curve can be extended to the ES-PFEM (5.11) for the motion of an open curve in solid-state dewetting. Again, the details are omitted here for brevity.*

6. Numerical results

In this section, we report numerical results of the performance of our proposed ES-PFEM (4.4) and (5.11) for the evolution of a closed curve and an open curve, respectively. We will test their spatial/temporal convergent rates and energy dissipation, and investigate their area/mass loss and mesh quality during the evolution.

To measure the difference between two curves Γ_1 and Γ_2 , we adopt the manifold distance $M(\Gamma_1, \Gamma_2)$ which was introduced in [31]. When Γ_1 and Γ_2 are two closed curves, let Ω_1 and Ω_2 be the regions enclosed by Γ_1 and Γ_2 , respectively; and when they are two open curves above the flat substrate, let Ω_1 and Ω_2 be the regions enclosed between the flat substrate and Γ_1 and Γ_2 , respectively. The manifold distance $M(\Gamma_1, \Gamma_2)$ is defined as [31] (cf. Figure 3):

$$M(\Gamma_1, \Gamma_2) := |(\Omega_1 \setminus \Omega_2) \cup (\Omega_2 \setminus \Omega_1)| = |\Omega_1| + |\Omega_2| - 2|\Omega_1 \cap \Omega_2|, \quad (6.1)$$

where $|\Omega|$ denotes the area of Ω .

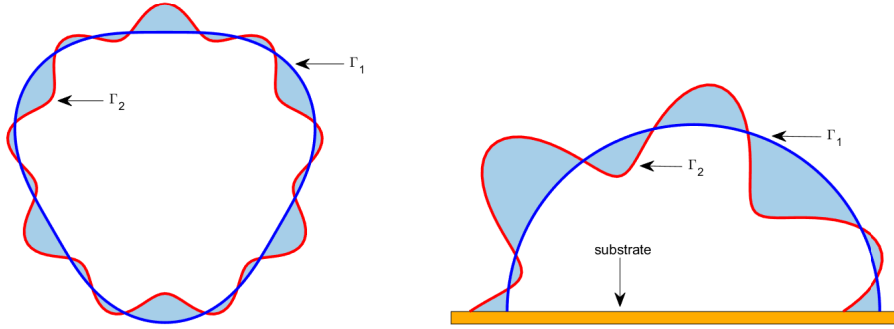


Figure 3: An illustration of the manifold distance $M(\Gamma_1, \Gamma_2)$. Two curves Γ_1 and Γ_2 are colored by blue and red, respectively, the substrate is colored by brown and $M(\Gamma_1, \Gamma_2)$ is defined as the area of the light blue region.

Suppose Γ^m is the numerical approximation of $\Gamma(t = t_m = m\tau)$ with mesh size h and time step τ under the choice of $\tau = h^2$, for simplicity, since formally our ES-PFEM is first order accurate in time and second order accurate in space. The numerical error is defined as

$$e^h(t_m) := M(\Gamma^m, \Gamma(t = t_m)), \quad m \geq 0, \quad (6.2)$$

where $\Gamma(t = t_m)$ is obtained numerically with a very small mesh size $h = h_e$ and a very small time step $\tau = \tau_e$, e.g. $h_e = 2^{-8}$ and $\tau_e = 2^{-16}$, in practical computations when the exact solution is not available. Let $A^h(t = t_m)$ be the area/mass of the region enclosed by Γ^m if it is a closed curve, and respectively, the region between the flat substrate and Γ^m if it is an open curve. Then the normized area/mass loss $\frac{\Delta A^h(t_m)}{A^h(0)}$ and the mesh ratio $R^h(t = t_m)$ which is used to measure the mesh quality of Γ^m , are defined as

$$\frac{\Delta A^h(t_m)}{A^h(0)} := \frac{A^h(t = t_m) - A^h(0)}{A^h(0)}, \quad R^h(t = t_m) := \frac{h_{\max}^m}{h_{\min}^m}, \quad m \geq 0, \quad (6.3)$$

where

$$h_{\max}^m := \max_{1 \leq j \leq N} |\mathbf{h}_j^m|, \quad h_{\min}^m := \min_{1 \leq j \leq N} |\mathbf{h}_j^m|, \quad m \geq 0.$$

In the following numerical simulations, the initial shapes are taken as a 4×1 rectangle for both closed curves and open curves except that they are stated otherwise. For solid-state dewetting problems, we always choose the contact line mobility $\eta = 100$ in (5.2) [31].

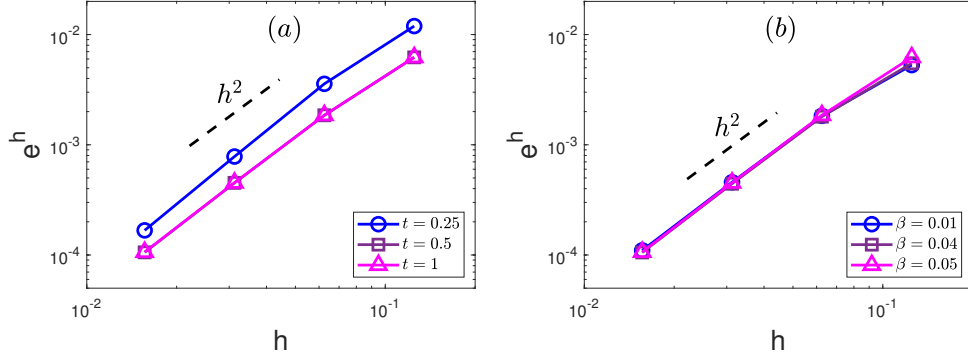


Figure 4: Plots of e^h vs h to test the spatial convergence rate of the ES-PFEM (4.4) with $\gamma(\theta) = 1 + \beta \cos(4\theta)$ for: (a) different times at $t = 0.25$, $t = 0.5$ and $t = 1$ with $\beta = 0.05$; and (b) different anisotropic strengths $\beta = 0.01$, $\beta = 0.04$ and $\beta = 0.05$ at time $t = 2$.

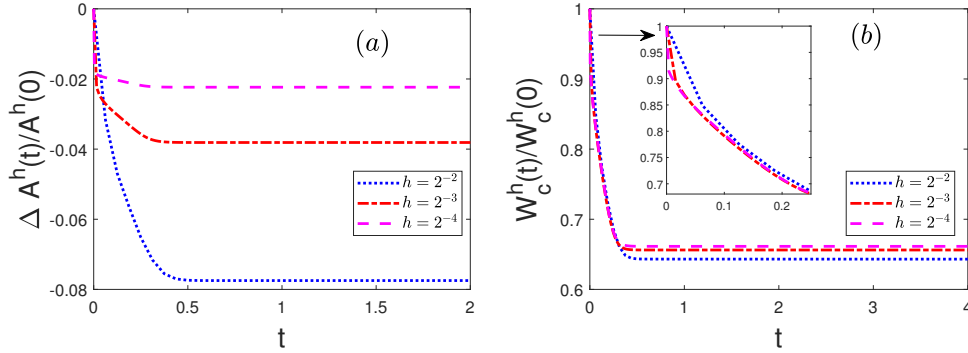


Figure 5: Time evolution of the normalized area/mass loss $\frac{\Delta A^h(t)}{A^h(0)}$ (left (a)) and the normalized energy $\frac{W_c^h(t)}{W_c^h(0)}$ (right (b)) for different mesh sizes h . The anisotropic surface energy is chosen as $\gamma = 1 + 0.05 \cos 4\theta$.

6.1. Results of the ES-PFEM (4.4) for the evolution of closed curves

Figure 4 plots spatial convergence rate of the ES-PFEM (4.4) with the anisotropic surface energy $\gamma(\theta) = 1 + \beta \cos(4\theta)$ for different times t and β . Figure 5 depicts the time evolution of the normalized area/mass loss $\frac{\Delta A^h(t_m)}{A^h(0)}$ and the energy dissipation $W_c^h(t_m)$ with $\gamma(\theta) = 1 + 0.05 \cos(4\theta)$ for different h . Finally Figure 6 shows the time evolution of the mesh ratio $R^h(t = t_m)$ with $\gamma(\theta) \equiv 1$ and $\gamma(\theta) = 1 + 0.05 \cos(4\theta)$ for different h .

From Figures 4-6, we can draw the following conclusions for the ES-PFEM (4.4) for the evolution of closed curves under anisotropic surface diffusion:

- (i) The ES-PFEM (4.4) is second order accurate in space and first order accurate in time (cf. Figure 4).
- (ii) It is unconditionally energy stable when the anisotropic surface energy $\gamma(\theta)$ satisfies those energy dissipation conditions in Section 3 (cf. Figure 5b).
- (iii) The mesh ratio $R^h(t = t_m)$ increases during a short period near $t = 0$ and then it decreases to a constant when $t \gg 1$. For isotropic surface energy, i.e. isotropic surface diffusion, $R^h(t = t_m) \rightarrow 1$ when $t \rightarrow +\infty$ (cf. Figure 6b), which indicates asymptotic mesh equal distribution (AMED) of the ES-PFEM (4.4) for isotropic surface diffusion. On the other hand, for anisotropic surface energy, i.e. anisotropic surface diffusion, $R^h(t = t_m) \rightarrow C > 1$ when $t \rightarrow +\infty$ (cf. Figure 6a), which indicates asymptotic mesh quasi-equal distribution (AMQD) of the ES-PFEM (4.4) for anisotropic surface diffusion.
- (iv) Area/mass loss is observed during a short period near $t = 0$, especially when the mesh size h is not small (cf. Figure 5a). When $t = t_m \gg 1$, area/mass is almost conserved and we observed numerically that

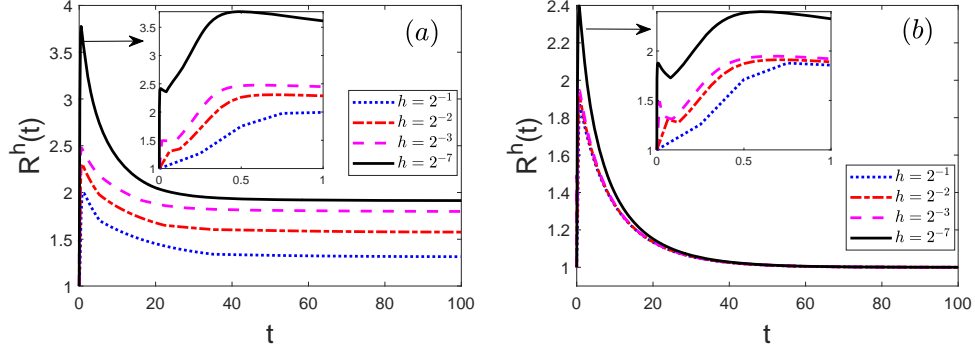


Figure 6: Time evolution of the mesh ratio $R^h(t)$ for different mesh sizes h with: (a) an anisotropic surface energy $\gamma(\theta) = 1 + 0.05 \cos 4\theta$; and (b) an isotropic surface energy $\gamma(\theta) \equiv 1$.

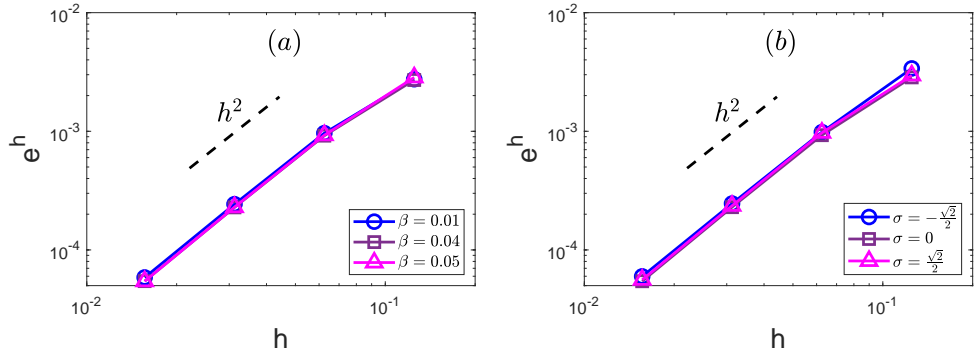


Figure 7: Plots of $e^h(t=2)$ vs h to test the spatial convergence rate of the ES-PFEM (5.11) with $\gamma(\theta) = 1 + \beta \cos(4\theta)$ for: (a) different β with $\sigma = 0$ in (5.4); (b) different σ in (5.4) with $\beta = 0.05$.

$|\frac{\Delta A^h(t_m)}{A^h(0)}| \leq Ch^2$, i.e. it converges quadratically and this agrees with the second order accuracy in space of the ES-PFEM (4.4).

6.2. Results of the ES-PFEM (5.11) for the evolution of open curves

Figure 7 plots spatial convergence rate of the ES-PFEM (5.11) with the anisotropic surface energy $\gamma(\theta) = 1 + \beta \cos(4\theta)$ for different times t and β . Figure 8 depicts the time evolution of the normalized area/mass loss $\frac{\Delta A^h(t_m)}{A^h(0)}$ and the energy dissipation $W_o^h(t_m)$ with $\gamma(\theta) = 1 + 0.05 \cos(4\theta)$ for different h . Finally Figure 9 shows the time evolution of the mesh ratio $R^h(t = t_m)$ with $\gamma(\theta) \equiv 1$ and $\gamma(\theta) = 1 + 0.05 \cos(4\theta)$ for different h .

Again, from Figures 7-9, we can draw the following conclusions for the ES-PFEM (5.11) for the evolution of open curves under anisotropic surface diffusion with applications in solid-state dewetting:

- (i) The ES-PFEM (5.11) is second order accurate in space and first order accurate in time (cf. Figure 7).
- (ii) It is unconditionally energy stable when the anisotropic surface energy $\gamma(\theta)$ satisfies those energy dissipation conditions in Section 3 (cf. Figure 8b).
- (iii) The mesh ratio $R^h(t = t_m)$ increases during a short period near $t = 0$ and then it decreases to a constant when $t \gg 1$. For isotropic surface energy, i.e. isotropic surface diffusion, $R^h(t = t_m) \rightarrow 1$ when $t \rightarrow +\infty$ (cf. Figure 9b), which indicates asymptotic mesh equal distribution (AMED) of the ES-PFEM (5.11) for isotropic surface diffusion. On the other hand, for anisotropic surface energy, i.e. anisotropic

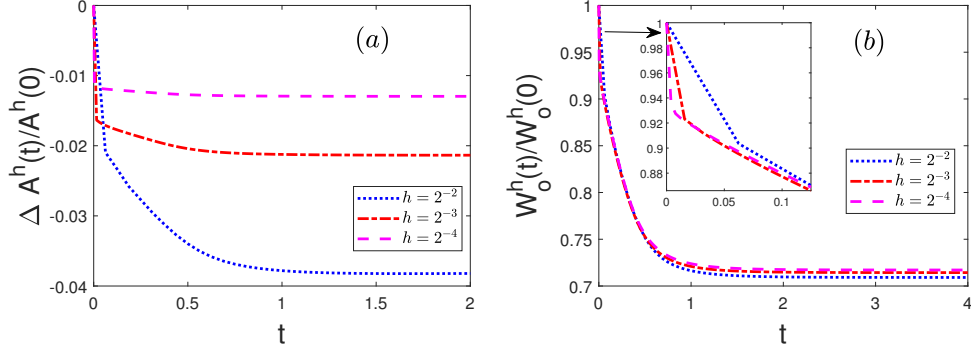


Figure 8: Time evolution of the normalized area/mass loss $\frac{\Delta A^h(t)}{A^h(0)}$ (left (a)) and the normalized energy $\frac{W_o^h(t)}{W_o^h(0)}$ (right (b)) for different mesh sizes h . The anisotropic surface energy is chosen as $\gamma = 1 + 0.05 \cos 4\theta$ and material constant $\sigma = -\frac{\sqrt{2}}{2}$ in (5.4).

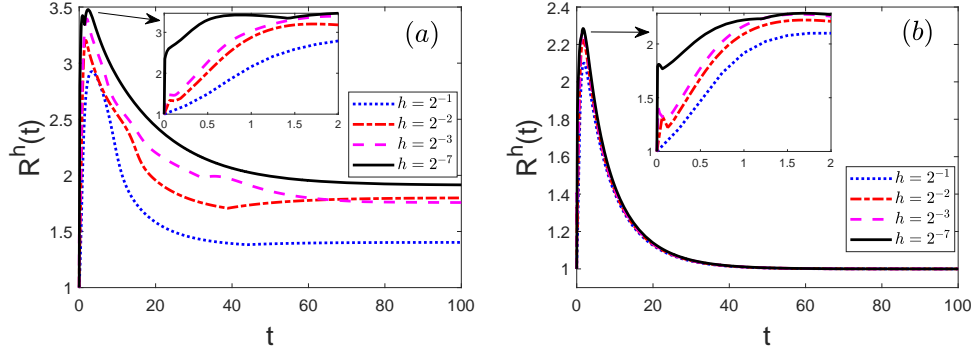


Figure 9: Time evolution of the mesh ratio $R^h(t)$ for different mesh sizes h with $\sigma = -\frac{\sqrt{2}}{2}$ in (5.4) and: (a) an anisotropic surface energy $\gamma(\theta) = 1 + 0.05 \cos 4\theta$; and (b) an isotropic surface energy $\gamma(\theta) \equiv 1$.

surface diffusion, $R^h(t = t_m) \rightarrow C > 1$ when $t \rightarrow +\infty$ (cf. Figure 9a), which indicates asymptotic mesh quasi-equal distribution (AMQD) of the ES-PFEM (5.11) for anisotropic surface diffusion.

(iv) Area/mass loss is observed during a short period near $t = 0$, especially when the mesh size h is not small (cf. Figure 8a). When $t = t_m \gg 1$, area/mass is almost conserved and we observed numerically that $|\frac{\Delta A^h(t_m)}{A^h(0)}| \leq Ch^2$, i.e. it converges quadratically and this agrees with the second order accuracy in space of the ES-PFEM (5.11).

6.3. Applications of the ES-PFEM for morphological evolution

Finally we examine the morphological evolution under different anisotropic surface energies by our proposed ES-PFEM. The morphological evolutions of closed curves and open curves from a 4×1 rectangle towards their equilibrium shapes are shown in Figure 10 and Figure 11, respectively. Four different anisotropic surface energies are taken as the isotropic energy $\gamma(\theta) \equiv 1$, the k -fold anisotropic energies $\gamma(\theta) = 1 + \frac{1}{1+3^2} \cos(3\theta) = 1 + \frac{1}{10} \cos(3\theta)$, $\gamma(\theta) = 1 + \frac{1}{1+4^2} \cos(4\theta) = 1 + \frac{1}{17} \cos(4\theta)$, and the ellipsoidal anisotropic energy $\gamma(\theta) = \sqrt{1 + \cos^2 \theta}$. For open curves, we take $\sigma = -\frac{\sqrt{2}}{2}$ in (5.4). From Corollaries 4.2 and 4.4, the parameters $a = 1$, $b = 1$ in $\gamma(\theta) = \sqrt{1 + \cos^2 \theta}$ attain the largest ratio $\frac{b}{a} = 1$ that we have proved for the ellipsoidal anisotropy, and the parameters $\beta = \frac{1}{1+3^2}, \beta = \frac{1}{1+4^2}$ are also the largest $\beta_{\max} = \frac{1}{1+k^2}$ for the k -fold anisotropy.

As observed from Fig. 10(a)-(d) and Fig. 11(a)-(d), the equilibrium shapes for the isotropic surface energy and the ellipsoidal anisotropic surface energy are indeed circle and ellipsis, respectively. As for k -

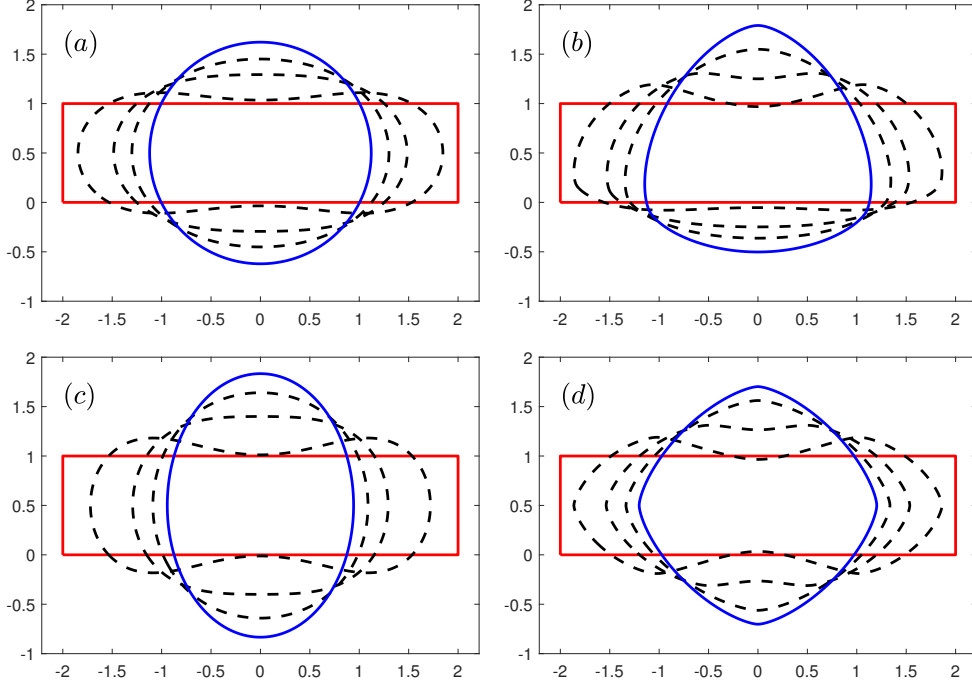


Figure 10: Morphological evolutions of a close rectangular curve under anisotropic surface diffusion with different anisotropic surface energies: (a) $\gamma(\theta) \equiv 1$, (b) $\gamma(\theta) = 1 + \frac{1}{10} \cos 3\theta$, (c) $\gamma(\theta) = \sqrt{1 + \cos^2 \theta}$, and (d) $\gamma(\theta) = 1 + \frac{1}{17} \cos 4\theta$. Other parameters are chosen as $h = 2^{-6}$, $\tau = h^2$. The red line is the initial shape, the black dashed lines are some snapshots during the evolution and the blue line is the equilibrium shape.

fold anisotropy, when k is changed from 3 to 4, the number of edges in their equilibrium shapes are also changed accordingly, as expected, which agree with both theoretical predictions and previous numerical results. Moreover, our ES-PFEM can handle the largest ratio $\frac{b}{a} = 1$ and the largest $\beta = \beta_{\max}$ well for both closed curves and open curves.

Our ES-PFEM also works well for different initial shapes including continuous but piecewise smooth initial curves. Figure 12 plots the morphological evolutions of four different closed initial configurations with k -fold anisotropy $\gamma(\theta) = 1 + \frac{1}{10} \cos(3\theta)$. We can see our ES-PFEM can handle successfully different initial curves with the same area, and the final equilibrium of different initial configurations is the same, which is consistent with the theoretical result.

Another three important quantities in morphological evolutions are the weighted curvature μ^m , the curvature κ^m , and the normal velocity $V^m := \mathbf{n}^m \cdot \frac{\mathbf{X}^{m+1} - \mathbf{X}^m}{\tau}$ which is an numerical approximation of $V(\cdot, t = t_m) = \partial_{ss}\mu(\cdot, t = t_m) = \mathbf{n} \cdot \partial_t \mathbf{X}|_{t=t_m}$. Notice that in our ES-PFEMs (4.4) and (5.11) for the evolution of a closed and open curve, respectively, we state how to compute numerically μ^m for $m \geq 1$, but we do not show how to compute numerically μ^0 and κ^m for $m \geq 0$. In fact, for a given closed initial configuration $\Gamma^0 = \mathbf{X}^0$ which might be continuous but only piecewise smooth such as a rectangle, one can adapt the following variational formulation to compute numerically $\mu^0 \in \mathbb{K}_p^h$ and $\kappa^m \in \mathbb{K}_p^h$:

$$\begin{aligned} (\mu^0, \mathbf{n}^0 \cdot \boldsymbol{\omega}^h)_{\Gamma^0}^h - (G(\theta^0) \partial_s \mathbf{X}^0, \partial_s \boldsymbol{\omega}^h)_{\Gamma^0}^h &= 0, \quad \forall \boldsymbol{\omega}^h \in \mathbb{X}_p^h, \\ (\kappa^m, \mathbf{n}^m \cdot \boldsymbol{\omega}^h)_{\Gamma^m}^h - (\partial_s \mathbf{X}^m, \partial_s \boldsymbol{\omega}^h)_{\Gamma^m}^h &= 0, \quad \forall \boldsymbol{\omega}^h \in \mathbb{X}_p^h, \quad m \geq 0. \end{aligned} \quad (6.4)$$

Similarly, for a given open initial configuration $\Gamma^0 = \mathbf{X}^0$, one needs to replace \mathbb{K}_p^h and \mathbb{X}_p^h by \mathbb{K}^h and \mathbb{X}^h , respectively. Figure 13 displays time evolution of the curvature $\kappa(t = t_m)$ at different times under isotropic

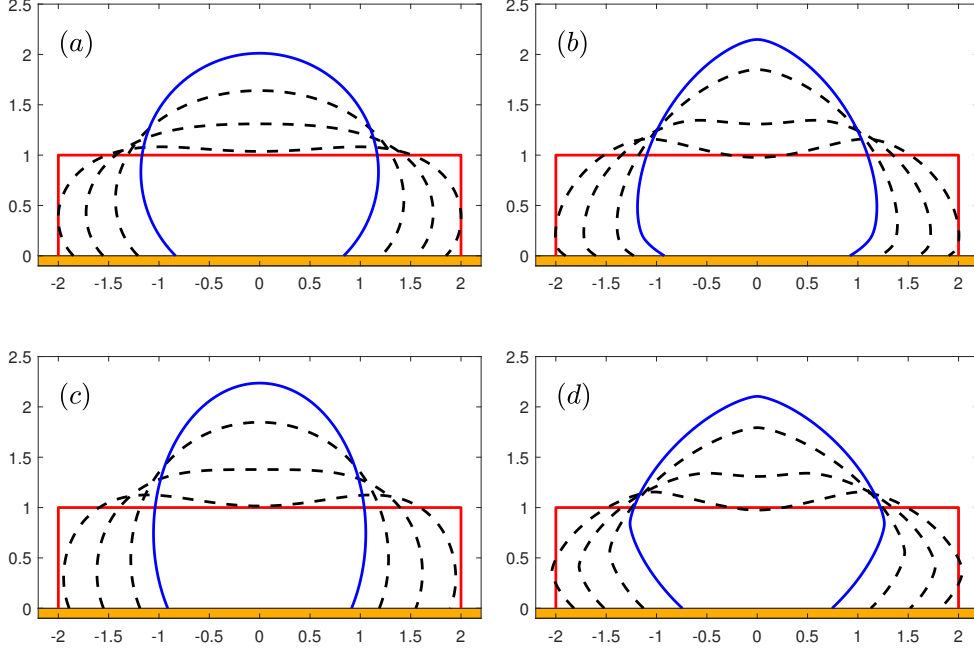


Figure 11: Morphological evolutions of an open rectangular curve under anisotropic surface diffusion with different anisotropic surface energies: (a) $\gamma(\theta) \equiv 1$, (b) $\gamma(\theta) = 1 + \frac{1}{10} \cos 3\theta$, (c) $\gamma(\theta) = \sqrt{1 + \cos^2 \theta}$, and (d) $\gamma(\theta) = 1 + \frac{1}{17} \cos 4\theta$. Other parameters are chosen as $\sigma = -\frac{\sqrt{2}}{2}$, $h = 2^{-6}$, $\tau = h^2$. The red line is the initial shape, the black dashed lines are some snapshots during the evolution, the blue line is the equilibrium shape and the brown base represents the substrate.

surface diffusion starting from an initial 2×2 square. Similarly, Figure 14 shows time evolution of the normal velocity $V(t = t_m)$ at different times under isotropic surface diffusion starting from an initial ellipse with length $2\sqrt{3}$ and width 2.

From Fig. 13, we can see that: (i) the curvature κ at the four sharp corners are discontinuous at $t = 0$, which are ‘numerically’ significant larger than those values of their neighbors (cf. Fig. 13a), (ii) after evolution of a few time steps with a small time step size τ , the sharp corners are being smoothed and the values of the curvature κ become comparable with those values of their neighbours (cf. Fig. 13b&c), and (iii) when the curve reaches its equilibrium shape, the curvature κ are almost the same at each point of the curve (cf. Fig. 13d).

7. Conclusions

By introducing a positive definite surface energy (density) matrix $G(\theta)$ depending on the anisotropic surface energy $\gamma(\theta)$, we obtained new and simple variational formulations for the motion of closed curves under anisotropic surface diffusion or open curves under anisotropic surface diffusion and contact line migration with applications in solid-state dewetting in materials science. We proved area/mass conservation and energy dissipation of the variational problems. The variational problems were first discretized in space by the parametric finite element method (PFEM) and then were discretized in time by an implicit/explicit (IMEX) backward Euler method. The full-discretization is semi-implicit and efficient since only a linear system needs to be solved at each time step. We identified different energy dissipation conditions on the anisotropic surface energy $\gamma(\theta)$ such that both the semi-discretization and full-discretization are unconditionally energy stable. Our numerical results suggested that the proposed energy-stable PFEM (ES-PFEM) has nice mesh quality – asymptotic mesh quasi-equal distribution – of the curves during their dynamics, i.e.

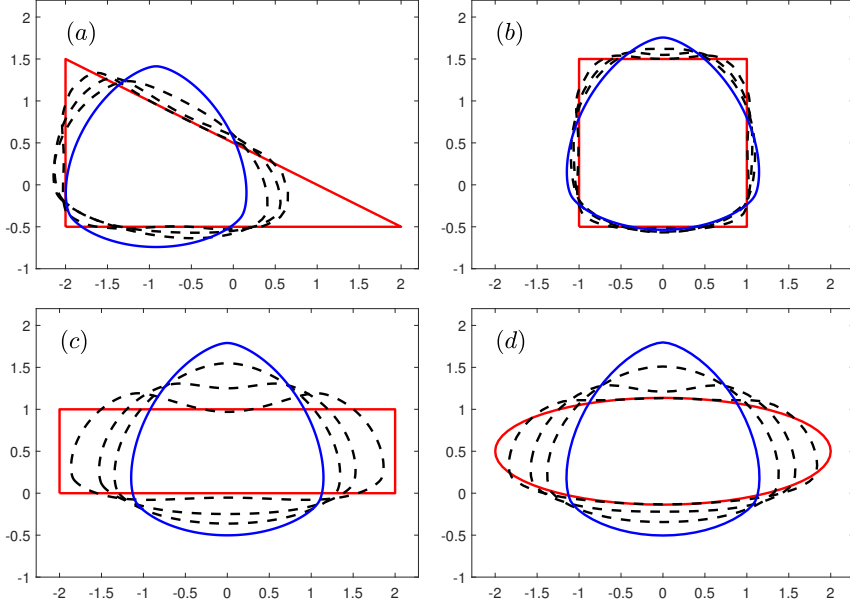


Figure 12: Morphological evolutions of different closed initial curves under anisotropic surface diffusion with anisotropic surface energy $\gamma(\theta) = 1 + \frac{1}{10} \cos(3\theta)$: (a) an initial 4×2 right triangle, (b) an initial 2×2 square, (c) an initial 4×1 rectangle, and (d) an initial ellipse with length 4 and width $\frac{4}{\pi}$. Other parameters are chosen as $h = 2^{-6}$, $\tau = h^2$. The red line is the initial shape, the black dashed lines are some snapshots during the evolution, the blue line is the equilibrium shape.

no re-meshing is needed during the simulation. In the future, we will extend the new variational formulation to anisotropic surface diffusion in three dimensions [20, 32] and other geometric flows arising from different applications.

Appendix A. Two trigonometric identities and their proof

Here we show two trigonometric identities which are used to prove Lemma B.1 in Appendix B.

Lemma A.1. $\forall n \in \mathbb{Z}^+$, $\forall \theta, \phi \in [-\pi, \pi]$, the following two trigonometric identities hold:

$$\sin(n\theta) - \sin(n\phi) - n \cos(n\theta) \sin(\theta - \phi) = (1 - \cos(\theta - \phi)) \left(n \sin(n\theta) + \sum_{l=1}^{n-1} 2l \sin(l\theta + (n-l)\phi) \right), \quad (\text{A.1})$$

$$\cos(n\theta) - \cos(n\phi) + n \sin(n\theta) \sin(\theta - \phi) = (1 - \cos(\theta - \phi)) \left(n \cos(n\theta) + \sum_{l=1}^{n-1} 2l \cos(l\theta + (n-l)\phi) \right). \quad (\text{A.2})$$

Proof. To prove (A.1), noticing the trigonometric identity

$$\cos \alpha \sin \beta = \frac{\sin(\alpha + \beta) - \sin(\alpha - \beta)}{2}, \quad (\text{A.3})$$

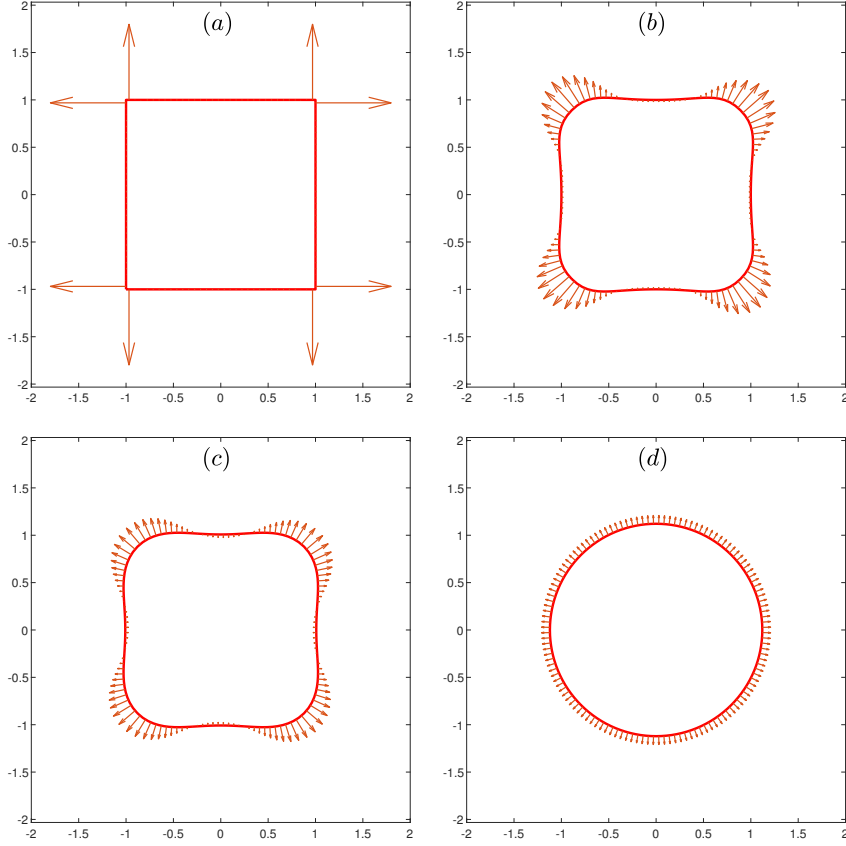


Figure 13: Time evolution of the curvature κ under isotropic surface diffusion at: (a) $t = 0$; (b) $t = \tau$; (c) $t = 3\tau$; (d) $t = 10^4\tau$, where mesh size $h = 2^{-5}$ and time step $\tau = h^2$. The initial curve is a 2×2 square. The length of the arrow in the figure is scaled as one-tenth of the actual κ .

subtracting the left hand side of (A.1) by its right hand side, we get

$$\begin{aligned}
& (1 - \cos(\theta - \phi)) \left(n \sin(n\theta) + \sum_{l=1}^{n-1} 2l \sin(l\theta + (n-l)\phi) \right) - [\sin(n\theta) - \sin(n\phi) - n \cos(n\theta) \sin(\theta - \phi)] \\
&= \sum_{l=1}^{n-1} 2l \sin(l\theta + (n-l)\phi) - \sum_{l=1}^{n-1} 2l \cos(\theta - \phi) \sin(l\theta + (n-l)\phi) + n \sin(n\theta) - n \cos(\theta - \phi) \sin(n\theta) \\
&\quad - \left[\sin(n\theta) - \sin(n\phi) - n \frac{\sin((n+1)\theta - \phi) - \sin((n-1)\theta + \phi)}{2} \right] \\
&= \sum_{l=1}^{n-1} 2l \sin(l\theta + (n-l)\phi) - \sum_{l=1}^{n-1} l \left[\sin((l+1)\theta + (n-l-1)\phi) + \sin((l-1)\theta + (n-l+1)\phi) \right] \\
&\quad + n \sin(n\theta) - n \frac{\sin((n+1)\theta - \phi) + \sin((n-1)\theta + \phi)}{2} \\
&\quad - \left[\sin(n\theta) - \sin(n\phi) - n \frac{\sin((n+1)\theta - \phi) - \sin((n-1)\theta + \phi)}{2} \right] \\
&= \sum_{l=1}^{n-1} 2l \sin(l\theta + (n-l)\phi) - \sum_{l=0}^{n-2} (l+1) \sin(l\theta + (n-l)\phi) - \sum_{l=2}^n (l-1) \sin(l\theta + (n-l)\phi) \\
&\quad + (n-1) \sin(n\theta) + \sin(n\phi) - n \sin((n-1)\theta + \phi) \\
&= 2(n-1) \sin((n-1)\theta + \phi) + 2 \sin(\theta + (n-1)\phi) - \sin(n\phi) - 2 \sin(\theta + (n-1)\phi) \\
&\quad - (n-1) \sin(n\theta) - (n-2) \sin((n-1)\theta + \phi) + (n-1) \sin(n\theta) + \sin(n\phi) - n \sin((n-1)\theta + \phi) \\
&= 0, \quad \forall \theta, \phi \in [-\pi, \pi], \tag{A.4}
\end{aligned}$$

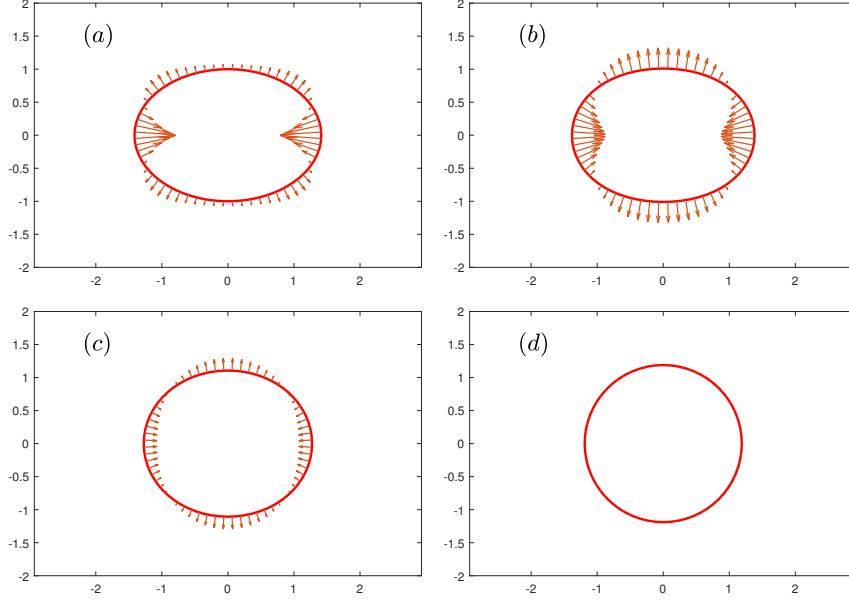


Figure 14: Time evolution of the normal velocity V under isotropic surface diffusion at: (a) $t = 0$; (b) $t = 20\tau$; (c) $t = 200\tau$; (d) $t = 10^4\tau$, where mesh size $h = 2^{-5}$ and time step $\tau = h^2$. The initial curve is an ellipse with length $2\sqrt{3}$ and width 2. The length of the arrow in the figure is scaled as one-tenth of the actual V for $t > 0$, and as one-twentieth of the actual V for $t = 0$.

which implies the trigonometric identity (A.1). Similarly, we can prove the second trigonometric identity (A.2) and the details are omitted here for brevity. \square

Appendix B. A trigonometric inequality and its proof

Here we prove a trigonometric inequality which is used to prove Theorem 4.3.

Lemma B.1. *The following trigonometric inequality holds:*

$$\begin{aligned} & a_n(\cos(n\theta) - \cos(n\phi) + n \sin(n\theta) \sin(\theta - \phi)) + b_n(\sin(n\theta) - \sin(n\phi) - n \cos(n\theta) \sin(\theta - \phi)) \\ & \geq -(1 - \cos(\theta - \phi))n^2 \sqrt{a_n^2 + b_n^2}, \quad \forall \theta, \phi \in [-\pi, \pi], \quad \forall n \in \mathbb{Z}^+. \end{aligned} \quad (\text{B.1})$$

Proof. Using (A.1) and (A.2), noticing that

$$1 - \cos(\theta - \phi) \geq 0, \quad a_n \cos n\theta + b_n \sin n\theta \geq -\sqrt{a_n^2 + b_n^2}, \quad \forall \theta, \phi \in [-\pi, \pi], \quad \forall n \in \mathbb{Z}^+,$$

we have

$$\begin{aligned} & a_n(\cos(n\theta) - \cos(n\phi) + n \sin(n\theta) \sin(\theta - \phi)) + b_n(\sin(n\theta) - \sin(n\phi) - n \cos(n\theta) \sin(\theta - \phi)) \\ & = a_n(1 - \cos(\theta - \phi)) \left(n \cos(n\theta) + \sum_{k=1}^{n-1} 2k \cos(k\theta + (n-k)\phi) \right) \\ & \quad + b_n(1 - \cos(\theta - \phi)) \left(n \sin(n\theta) + \sum_{k=1}^{n-1} 2k \sin(k\theta + (n-k)\phi) \right) \\ & \geq -(1 - \cos(\theta - \phi)) \left(n + \sum_{k=1}^{n-1} 2k \right) \sqrt{a_n^2 + b_n^2} \\ & = (1 - \cos(\theta - \phi))n^2 \sqrt{a_n^2 + b_n^2}, \quad \forall \theta, \phi \in [-\pi, \pi], \quad \forall n \in \mathbb{Z}^+, \end{aligned} \quad (\text{B.2})$$

which implies the desired inequality (B.1). \square

Acknowledgement

This work was supported by the Academic Research Fund of the Ministry of Education of Singapore grant No. MOE2019-T2-1-063 (R-146-000-296-112). Part of the work was done when the authors were visiting the Institute of Mathematical Science at the National University of Singapore in 2020.

References

References

- [1] R. A. Adams and J. J. Fournier, Sobolev Spaces, Elsevier, 2003.
- [2] E. Bänsch, P. Morin, and R. H. Nochetto, A finite element method for surface diffusion: the parametric case, *J. Comput. Phys.* 203 (2005) 321-343.
- [3] W. Bao, W. Jiang, Y. Wang, and Q. Zhao, A parametric finite element method for solid-state dewetting problems with anisotropic surface energies, *J. Comput. Phys.* 330 (2017) 380-400.
- [4] W. Bao, W. Jiang, D. J. Srolovitz, and Y. Wang, Stable equilibria of anisotropic particles on substrates: a generalized Winterbottom construction, *SIAM J. Appl. Math.* 77 (2017) 2093-2118.
- [5] W. Bao and Q. Zhao, A structure-preserving parametric finite element method for surface diffusion, *SIAM J. Numer. Anal.*, to appear (arXiv: 2104.01432).
- [6] J. W. Barrett, H. Garcke, and R. Nürnberg, A parametric finite element method for fourth order geometric evolution equations, *J. Comput. Phys.* 222 (2007) 441-467.
- [7] J. W. Barrett, H. Garcke, R. Nürnberg, On the variational approximation of combined second and fourth order geometric evolution equations, *SIAM J. Sci. Comput.* 29 (2007) 1006-1041.
- [8] J. W. Barrett, H. Garcke, and R. Nürnberg, Numerical approximation of anisotropic geometric evolution equations in the plane, *IMA J. Numer. Anal.* 28 (2008) 292-330.
- [9] J. W. Barrett, H. Garcke, and R. Nürnberg, A variational formulation of anisotropic geometric evolution equations in higher dimensions, *Numer. Math.* 109 (2008) 1-44.
- [10] J. W. Barrett, H. Garcke, and R. Nürnberg, Finite element methods for fourth order axisymmetric geometric evolution equations, *J. Comput. Phys.* 376 (2019) 733-766.
- [11] J. Cahn, Stability, microstructural evolution, grain growth, and coarsening in a two-dimensional two-phase microstructure, *Acta. Mater.* 39 (1991) 2189-2199.
- [12] J.W. Cahn, J.E. Taylor, Surface motion by surface diffusion, *Acta Metall. Mater.* 42 (1994) 1045-1063.
- [13] U. Clarenz, U. Diewald, and M. Rumpf, Anisotropic geometric diffusion in surface processing, *IEEE Proceedings Visualization* (2000) 397-405.
- [14] F. Davi and M. E. Gurtin, On the motion of a phase interface by surface diffusion, *Z. Angew. Math. Phys.* 41 (1990) 782-811.
- [15] G. Dziuk, An algorithm for evolutionary surfaces, *Numer. Math.* 58 (1990) 603-611.
- [16] F. Haußer and A. Voigt, A discrete scheme for parametric anisotropic surface diffusion, *J. Sci. Comput.* 30 (2007) 223-235.
- [17] W. Jiang, W. Bao, C. V. Thompson and D. J. Srolovitz, Phase field approach for simulating solid-state dewetting problems, *Acta Mater.* 60 (2012) 5578-5592.
- [18] W. Jiang and B. Li, A perimeter-decreasing and area-conserving algorithm for surface diffusion flow of curves, arXiv: 2102.00374.
- [19] W. Jiang, Y. Wang, Q. Zhao, D. J. Srolovitz, and W. Bao, Solid-state dewetting and island morphologies in strongly anisotropic materials, *Scr. Mater.* 115 (2016) 123-127.
- [20] W. Jiang, Q. Zhao and W. Bao, Sharp-interface model for simulating solid-state dewetting in three dimensions, *SIAM J. Appl. Math.* 80 (2020) 1654-1677.
- [21] Z. Li, H. Zhao, and H. Gao, A numerical study of electro-migration voiding by evolving level set functions on a fixed cartesian grid, *J. Comput. Phys.* 152 (1999) 281-304.
- [22] W. W. Mullins, Theory of thermal grooving, *J. Appl. Phys.* 28 (1957) 333-339.
- [23] K. Oura, V. G. Lifshits, A. A. Saranin, A. V. Zotov, and M. Katayama, *Surface Science: An Introduction*, Springer-Verlag, Berlin Heidelberg, 2003.
- [24] P. Pozzi, Anisotropic mean curvature flow for two-dimensional surfaces in higher codimension: a numerical scheme, *Interface Free Bound.* 10 (2008) 539-576.
- [25] E. Shustorovich, *Metal-Surface Reaction Energetics: Theory and Applications to Heterogeneous Catalysis, Chemisorption, and Surface Diffusion*, VCH Publishers Inc., 1991.
- [26] D. J. Srolovitz, S. A. Safran, Capillary instability in thin films. II. kinetics, *J. Appl. Phys.* 60 (1986) 255-260.
- [27] J. E. Taylor and J. W. Cahn, Linking anisotropic sharp and diffuse surface motion laws via gradient flows, *J. Stat. Phys.* 77 (1994) 183-197.
- [28] C. V. Thompson, Solid state dewetting of thin films, *Annu. Rev. Mater. Res.* 42 (2012) 399-434.
- [29] Y. Wang, W. Jiang, W. Bao, and D. J. Srolovitz, Sharp interface model for solid-state dewetting problems with weakly anisotropic surface energies, *Phys. Rev. B* 91 (2015) 045303.
- [30] J. Ye, C. V. Thompson, Mechanisms of complex morphological evolution during solid-state dewetting of single-crystal nickel thin films, *Appl. Phys. Lett.* 97 (2010) 071904.

- [31] Q. Zhao, W. Jiang, and W. Bao, An energy-stable parametric finite element method for simulating solid-state dewetting, *IMA J. Numer. Anal.* 41 (2021) 2026-2055.
- [32] Q. Zhao, W. Jiang and W. Bao, A parametric finite element method for solid-state dewetting problems in three dimensions, *SIAM J. Sci. Comput.* 42 (2020) B327-B352.